Oxide ionic conduction in Bi_2O_3 and its solid solutions

Kazuki Shitara

2015

Contents

Chapter 1

General Introduction

Oxide ionic conductors have been used as oxygen sensors, solid oxide fuel cells and oxygen separation membranes [1,2]. Bismuth sesquioxide with a cubic form, δ-Bi_2O_3, is one of oxide materials with a high oxide ionic conductivity. The δ-Bi_2O_3 shows oxygen conductivity of nearly 1 S/cm at high temperatures better than that of yttria stabilized zirconia (YSZ) [3,4]. This high ionic conductivity has been revealed to originate from the crystal structure of the δ-Bi_2O_3. The δ-Bi_2O_3 has a defective fluorite structure, where empty oxygen sites are distributed randomly for the charge neutrality [5–9]. The disordering on the oxygen sublattice is related to its high ionic conductivity, which is examined by first-principles molecular dynamics simulations [8,9]. However, the δ phase is stable only in the temperature range between 1002 K and melting point of 1097 K. The phase transition from the δ phase to α or β phase is reported to involve a dramatic decrease of the oxygen conductivity [3,10].

The use of a solid solution of Bi_2O_3 and some rare-earth oxides has been known as a method to stabilize the δ phase at room temperature [11]. For instance, an erbium oxide stabilized δ-Bi_2O_3, especially Er_2O_3 20 mol% doped Bi_2O_3 among them, shows a high ionic conductivity nearly equal to that of pure δ-Bi_2O_3 at high temperatures [12]. At the same time, it shows a deflection of ionic conductivity at middle temperature range about 800 K as shown in Figure 1 and this deflection is observed in a solid solution with some other rare-earth oxides as well [13,14]. The ionic conductivity at room temperature is much lower than that expected from a simple Arrhenius extrapolation of the high temperature data. The origin of the deflection of the ionic conductivity is not clearly understood, while a natural presumption that the deflection is ascribed to the ordering on the oxygen sublattice can be derived. Based on this presumption, the order-disorder transition temperature controls the ionic conductivity at low temperatures. To obtain a system with a high ionic conductivity, it is necessary to find a system with a low order-disorder transition temperature.

In chapter 2, the order-disorder transition temperatures T_c of oxide sublattice in eight kinds of Bi_2O_3-M_2O_3 systems (M=La, Nd, Sm, Gd, Dy, Y, Er, Lu) are systematically predicted from the density functional theory (DFT) calculation [15,16]. We here use a concise method to predict the order-disorder transition temperature. In this approach, the order-disorder transition temperature is estimated by calculating the free energies of most stable ordered structures and perfectly disordered structures. The ordered structures are explored by an analysis of the correlation functions defined in the cluster expansion method [17,18].

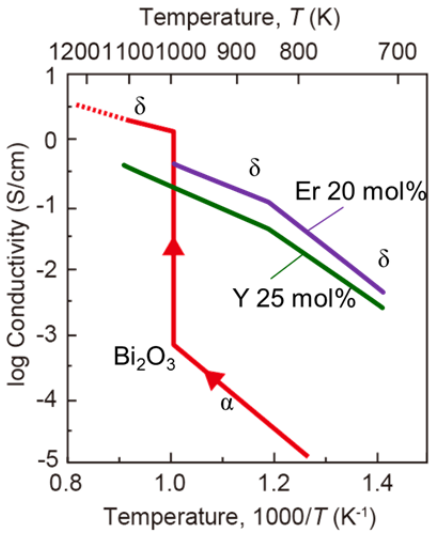

Figure 1. Ionic conductivity of pure Bi_2O_3, Er_2O_3-20% Bi_2O_3 and Y_2O_3-25mol% Bi_2O_3

Moreover, the conductivity at higher temperature than deflection points becomes lower with the increase of the solutes concentration. Figure 2 shows the ionic conductivity in Bi_2O_3-Y_2O_3 system [14] and the decrease of ionic conductivity is observed with increasing of Y_2O_3 concentration. This tendency is observed in other solutes, Er, Dy, and Gd [12,13,19] as well. There are few reports about oxygen diffusion mechanism of a solid solution of Bi_2O_3 and some rare-earth oxides. M. Yashima reported the structure of the ytterbium substituted system $Bi_{1.4}Yb_{0.6}O_3$ [20]. In this report, the cation sublattice is also disordered and oxygen diffuses just the same as pure Bi_2O_3. M. Krynski reported that yttrium traps oxygen and disrupts oxygen diffusions in δ-Bi_3YO_6 by first-principles molecular dynamics [21]. The effects on the ionic conductivity of alloying with rare-earth elements are not clearly revealed for various rare-earth elements. In order to investigate the origin of the decrease of ionic conductivity, it is considered to be useful to construct and analyze the systematic database of ionic conductivity. Although the exhaustive database can be constructed by the first-principles molecular dynamics, however, it is hardly cheap to calculate exhaustive systems. In addition, it is useful to predict the conductivity of other systems without molecular dynamics. For this purpose, the analyses of information science will be helpful. There are two purposes using the information science technology. One is a discovery of the relationship we have never found. The other is the prediction of ionic conductivity without experiments or heavy calculations.

In chapter 3, first-principles molecular dynamics simulations of eight kinds of Bi_2O_3-M_2O_3 systems (M=La, Nd, Sm, Gd, Dy, Y, Er, Lu) were performed at several temperatures. After molecular dynamics simulations, self-diffusion coefficients and two types of distribution functions, angular and radial, were calculated. Temperature and composition dependence of them was investigated. Furthermore, the informatics analyses were performed to find the relationship between parameters and to predict the material property, diffusion coefficients.

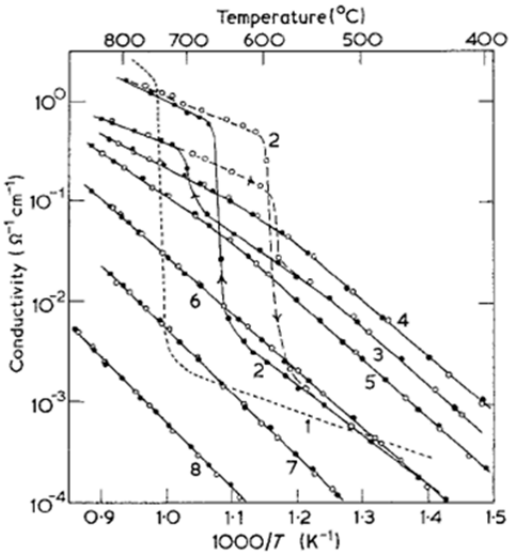

Figure 2. Reported conductivity in $(Bi_2O_3)_{1-x}(Y_2O_3)_x$ [14]. The values for x are: 1-0; 2-0.05; 3-0.20; 4-0.25; 5-0.33; 6-0.425; 7-0.50; 8-0.60.

References

[1] A. M. Azad, S. Larose, and S. A. Akbar, J. Mater. Sci. **29**, 4135 (1994).

[2] P. Knauth and H. Tuller, J. Am. Ceram. Soc. **80**, 1654 (2002).

[3] H. A. Harwig and A. G. Gerards, Thermochim. Acta **28**, 121 (1979).

[4] T. Takahashi and H. Iwahara, Mater. Res. Bull. **13**, 1447 (1978).

[5] G. Gattow and D. Schütze, Zeitschrift Für Anorg. Und … **546**, (1964).

[6] P. D. Battle and C. R. A. Catlow, J. Phys. C: Solid State Phys. **16**, L561 (1983).

[7] M. Yashima and D. Ishimura, Chem. Phys. Lett. **378**, 395 (2003).

[8] C. Mohn, S. Stølen, S. Norberg, and S. Hull, Phys. Rev. Lett. **102**, 100 (2009).

[9] A. Seko, Y. Koyama, A. Matsumoto, and I. Tanaka, J. Phys. Condens. Matter **24**, 475402 (2012).

[10] P. Shuk, H. D. Wiemhöfer, U. Guth, W. Göpel, and M. Greenblatt, Solid State Ionics **89**, 179 (1996).

[11] N. Sammes, G. Tompsett, H. Nafe, and F. Aldinger, J. Eur. Ceram. Soc. **19**, (1999).

[12] M. Verkerk and K. Keizer, J. Appl. Electrochem. **10**, (1980).

[13] T. Takahashi, T. Esaka, and H. Iwahara, J. Appl. Electrochem. **5**, 197 (1975).

[14] T. Takahashi, H. Iwahara, and T. Arao, J. Appl. Electrochem. **5**, 187 (1975).

[15] P. Hohenberg and W. Kohn, Phys. Rev. **155**, (1964).

[16] W. Kohn and L. Sham, Phys. Rev. **385**, (1965).

[17] G. L. W. Hart, Nat. Mater. **6**, 941 (2007).

[18] K. Fujimura, A. Seko, Y. Koyama, A. Kuwabara, I. Kishida, K. Shitara, C. A. J. Fisher, H. Moriwake, and I. Tanaka, Adv. Energy Mater. **3**, 980 (2013).

[19] M. J. Verkerk and A. J. Burggraaf, J. Electrochem. Soc. **128**, 75 (1981).

[20] M. Yashima and D. Ishimura, Appl. Phys. Lett. **87**, 221909 (2005).

[21] M. Krynski, W. Wrobel, C. E. Mohn, J. R. Dygas, M. Malys, F. Krok, and I. Abrahams, Solid State Ionics **264**, 49 (2014).

Chapter 2

Prediction of Order-disorder Transition Temperature of Oxygen Sublattice in Bismuth and Rare-earth Oxides Solution by Systematic First-principles Calculations

1. Introduction

Oxide ionic conductors have been used as oxygen sensors, solid oxide fuel cells and oxygen separation membranes [1,2]. Bismuth sesquioxide with a cubic form, δ-Bi_2O_3, is one of oxide materials with a high oxide ionic conductivity. The δ-Bi_2O_3 shows oxygen conductivity of nearly 1 S/cm at high temperatures better than that of yttria stabilized zirconia [3,4]. This high ionic conductivity has been revealed to originate from the crystal structure of the δ-Bi_2O_3. The δ-Bi_2O_3 has a defective fluorite structure, where empty oxygen sites are distributed randomly for the charge neutrality [5–10]. The disordering on the oxygen sublattice is related to its high ionic conductivity, which is examined by first-principles molecular dynamics simulations [10,11]. However, the δ phase is stable only in the temperature range between 1002 K and melting point of 1097 K. The phase transition from the δ phase to α or β phase is reported to involve a dramatic decrease of the oxygen conductivity [3,12].

The use of a solid solution of Bi_2O_3 and some rare-earth oxides has been known as a method to stabilize the δ phase at room temperature [13]. For instance, an erbium oxide stabilized δ-Bi_2O_3, especially Er_2O_3 20 mol% doped Bi_2O_3 among them, shows a high ionic conductivity nearly equal to that of pure δ-Bi_2O_3 at high temperatures [14]. At the same time, it shows a deflection of ionic conductivity at middle temperature range about 800 K [14–16] as shown in Figure 1. The ionic conductivity at room temperature is much lower than that obtained from a simple Arrhenius extrapolation of the high temperature data. The origin of the deflection of the

ionic conductivity is not clearly understood, while a natural presumption that the deflection is ascribed to the ordering on the oxygen sublattice can be derived. Based on this presumption, the order-disorder transition temperature controls the ionic conductivity at low temperatures. To obtain a system with a high ionic conductivity, it is necessary to find a system with a low order-disorder transition temperature.

In this study, the order-disorder transition temperatures T_c in eight kinds of Bi_2O_3-M_2O_3 systems (M=La, Nd, Sm, Gd, Dy, Y, Er, Lu) are systematically predicted from the density functional theory (DFT) calculation [17,18]. To accurately predict the order-disorder transition temperature in multicomponent systems, the DFT calculation is generally combined with the cluster expansion (CE) method [19–21] and Monte Carlo (MC) simulation. In this framework, an effective Hamiltonian describing accurately the energetics of the multicomponent system is constructed from a systematic set of DFT calculations for ordered structures, and then the order-disorder transition temperature is estimated from systematic MC simulations using a fine interval of the temperature and chemical potential. Instead of performing the complete CE, we here use a concise method to predict the order-disorder transition temperature. In this approach, the order-disorder transition temperature is estimated by calculating the free energies of stable ordered structures and perfectly disordered structures. The ordered structures are explored by an analysis of the correlation functions defined in the cluster expansion method [22,23].

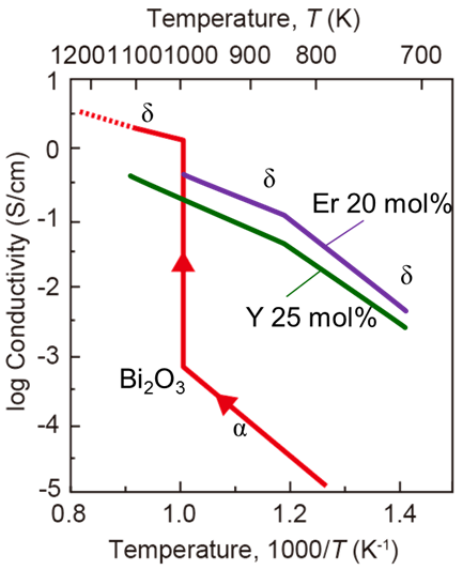

Figure 1. Ionic conductivity of pure Bi_2O_3, Er_2O_3-20% Bi_2O_3 and Y_2O_3-25mol% Bi_2O_3

2. Ordered and disordered structures of Bi_2O_3-M_2O_3

Figure 2 shows the unit cell of the fluorite structure of Bi_2O_3-M_2O_3 considered in this study. The fluorite structure can be divided into octants, whose centers are 8c sites. Cation and 8c sites form face-centered cubic (fcc) and simple cubic lattices, respectively. In the δ-Bi_2O_3, the total occupancy of oxygen atoms in an octant is 3/4 because a quarter of octants are empty and oxygen atoms are disordered. In addition, each octant also has four 32f sites as shown in Figure 3. Although it is suggested that not only the 8c but also the 32f sites are occupied by oxygen atoms in δ-Bi_2O_3 from the analysis of neutron diffraction experiments [7] and first-principles molecular dynamics calculations [10], an approximation that configurations of oxygen atoms on the 32f sites are not considered is introduced here. Using this approximation, for ordered structures of Bi_2O_3-M_2O_3 pseudobinary system, the most stable structure for each composition is explored by considering both cation configurations on the cation sublattice and anion configurations on the 8c sublattice. For disordered structures, both the disordering of cations on the cation sublattice and the disordering of anions on the 8c sublattice are considered.

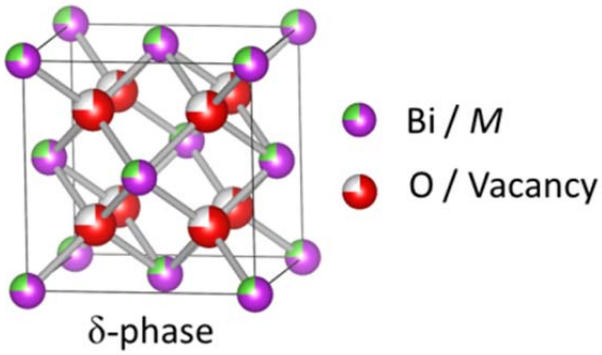

Figure 2. Structure of δ-Bi_2O_3-M_2O_3. It has two sublattiaces, cation (bismuth and rare earth element *M*) and anion (oxygen and vacancy). This figure was drawn by VESTA code [24].

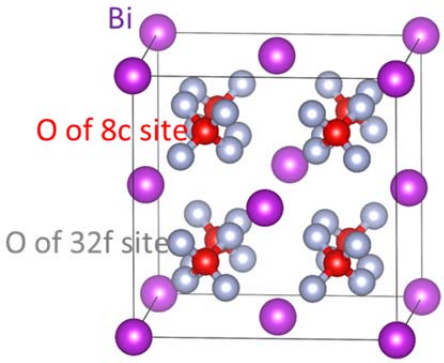

Figure 3. Structure of δ-Bi_2O_3. Each octant has four 32f sites partially occupied by oxygen. This figure was drawn by VESTA code [24].

3. Energies of disordered structures

To calculate the energy of perfectly disordered structure, two methods were examined. One is the special quasirandom structures (SQSs) [25] and the other is to average the energies of random structures. Both methods depend on the equation of cluster expansion (CE) method. In the CE method, the configurational energy E of a binary system is expressed as

$$E = V_0 + \sum_i V_i\sigma_i + \sum_{i,j} V_{ij}\sigma_i\sigma_j + \sum_{i,j,k} V_{ijk}\sigma_i\sigma_j\,\sigma_k + \cdots, \quad (1)$$

where σ_i and V denote the spin variable for respective site i and effective cluster interaction, respectively. This equation can be summarized as

$$E = \sum_\alpha V_\alpha\varphi_\alpha\,, \quad (2)$$

where φ_α is the correlation function of cluster α. A set of the correlation functions describes the atomic configuration. The SQSs are the structures which mimic the correlation functions of a perfectly disordered structure, $\varphi_\alpha(\mathrm{disorder})$. The correlation functions of the perfectly disordered structure can be analytically obtained according to its composition.

In this study, three types of SQSs were considered. The first type of SQSs was decided by the root mean squared difference between the correlation functions of a candidate structure and those of the purely disordered structure, $\varphi_\alpha(\mathrm{disorder})$, as

$$\Phi = \sqrt{\frac{1}{n}\sum_\alpha\{\varphi_\alpha - \varphi_\alpha(\mathrm{disorder})\}^2} \quad (3)$$

where n means the number of considered clusters. These SQSs were searched exhaustively in all configurations within 20 atoms of δ-Bi_2O_3-M_2O_3. These SQSs were called as "SQS-exh.-RMS", because they were searched exhaustively and the root mean square, Φ was used as criteria. The second one is also searched exhaustively but different in the view point of criteria. The values of $\varphi_\alpha - \varphi_\alpha(\mathrm{disorder})$ are used as criteria and the SQSs were selected to have many values of $\varphi_\alpha - \varphi_\alpha(\mathrm{disorder})$ equal to zero, i.e. the correlation function of the cluster α is same as a perfect disordered structure. These SQSs were called as "SQS-exh.-0". Third one is made by simulated annealing. Although exhaustive search should be performed if possible, this method is applied when exhaustive search is impossible because of large cell size. These SQSs were called as "SQS-S.A." The enumeration of possible configurations and calculation

of their correlation functions are performed by the CLUPAN code [26].

Another method is averaging the energies of random structures to expect that the correlation functions are averaged to be close to the correlation functions of the purely disordered structure. If a structure is picked up randomly, this structure is likely to have close values of the correlation functions of a perfectly disordered structure because of the distribution in the correlation function space shown in Figure 4. Averaging many random structures, the correlation functions are expected to be closer to that of a perfectly disordered structure.

In this section, these four methods, three types of SQSs and averaging random structures, were compared and applied to 12.5 mol% and 25 mol% Y_2O_3 doped Bi_2O_3 systems. The SQSs which are searched exhaustively were selected from all configurations within 20 atoms considering the 5th nearest neighbor pairs of anion sublattice, cation sublattice, and the cross term of them. SQS-S.A. is found from 2×2×2 supercell of fluorite unit cell considering the 3rd nearest neighbor pairs of anion sublattice, cation sublattice, and the cross term of them. The root mean square, Φ is used as criteria in SQS-S.A. When averaging the energies of random structures, the 2×2×2 supercell of fluorite unit cell is considered, as well. The values $\varphi_\alpha - \varphi_\alpha(\text{disorder})$ of the selected structures in 12.5 mol% and 25 mol% are shown in Table 1 and Table 2, respectively.

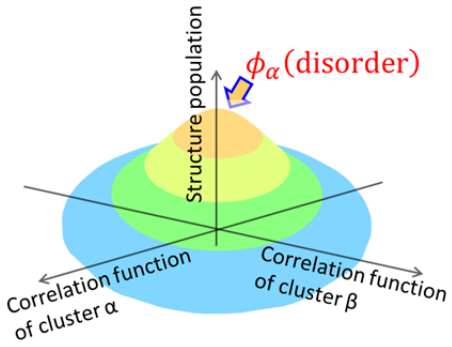

Figure 4. Schematic illustration of structure population in two dimensional correlation function space. The peak top is at the value of correlation function of the disordered structure.

Table 1. Values of $\varphi_\alpha - \varphi_\alpha(\text{disorder})$ of selected structures as SQSs in 12.5 mol% doped system. The value of zero means that the structure mimics the perfectly disordered structure well.

	N-th nearest pair	SQS -exh.-RMS			SQS-exh.-0					SQS-S. A.		
Anion sublattice Oxygen - Vacancy	1st	0	0	0	0	0	0	0	0	0.25	0.25	0.25
	2nd	0	0	0	0	0	0	0	0	0.083	0.083	0.083
	3rd	0	0	0	0	0	0	0	0	0.25	0.25	0.25
	4th	0	0	0	0	0	0	0	0	-0.25	-0.25	-0.25
	5th	-0.083	-0.083	-0.083	0.167	0.083	0.167	0.083	0.083	-0.25	-0.25	-0.25
Cation sublattice Bismuth - Rare earth	1st	0.021	-0.063	-0.063	-0.063	-0.063	-0.063	-0.063	-0.063	0	0	-0.021
	2nd	-0.063	-0.063	-0.063	0.104	0.104	0.104	0.104	0.104	0.021	0.021	0.021
	3rd	-0.063	0.021	0.021	0.021	0.021	0.021	-0.063	-0.063	-0.021	-0.021	0
	4th	0.021	0.021	0.021	-0.063	-0.063	-0.063	0.104	0.104	-0.063	-0.063	-0.063
	5th	0.021	0.021	0.021	-0.063	-0.063	-0.063	-0.063	-0.063	0	0	-0.021
The cross term Anion sublattice - Cation sublattice	1st	0	0	0	0	0	0	0	0	0.063	0.063	0.063
	2nd	-0.021	0.021	-0.021	0	0	0	0	0	0.042	0.042	0.042
	3rd	0.042	-0.021	0.021	0	0	0	0	0	-0.021	-0.021	-0.021
	4th	0.021	-0.021	0.021	0	0	0	0	0	0.042	0.042	0.042
	5th	0.063	0	0	0	0	0	0	0	-0.125	-0.125	-0.125

Table 2. Values of $\varphi_\alpha - \varphi_\alpha(\text{disorder})$ of selected structures as SQSs in 25 mol% doped system. The value of zero means that the structure mimics the perfectly disordered structure well.

	N-th nearest pair	SQS-exh.-RMS						SQS-exh.-0		SQS-S. A.		
Anion sublattice Oxygen - Vacancy	1st	0.083	0.083	0.083	0	0	0	-0.083	0	0	0	0
	2nd	-0.083	-0.083	-0.083	0.042	0	0	-0.083	0	0	0	0
	3rd	0.25	-0.25	0	0	0	0	-0.25	0	0	0	0
	4th	0.25	-0.25	-0.25	0	0	0	0.75	0	-0.063	-0.125	-0.031
	5th	0.083	0.083	-0.25	-0.083	0.083	0.083	-0.25	0.083	0.125	-0.167	-0.042
Cation sabulattice Bismuth - Rare earth	1st	-0.083	-0.083	-0.083	0.083	-0.083	-0.083	-0.083	-0.083	0	0	0
	2nd	0.083	0.083	-0.25	-0.083	0.083	0.083	-0.25	-0.25	0	0	0
	3rd	-0.083	-0.083	0	-0.083	-0.083	-0.083	-0.083	0	0	0	0
	4th	0.083	0.083	0.25	-0.083	0.083	0.083	0.75	0.25	-0.25	-0.25	-0.25
	5th	-0.083	-0.083	0.083	-0.083	-0.083	-0.083	-0.083	0.083	0	0	0
The cross term Anion sublattice - Cation sublattiace	1st	0	0.125	0.125	0	0	0	0	0	0	0	0
	2nd	0	-0.042	-0.083	0	0	0	0	0	0	0	0
	3rd	0	-0.042	-0.042	0.021	0	0	0	0	0	0	0
	4th	0	-0.042	0.083	0.021	0	0	0	0	0	0	0
	5th	0	0.125	0	-0.063	0	0	0	0	0	0	0

The relative energies in Y_2O_3 12.5 mol% are shown in Figure 5. The error of 0.1 eV / $Bi_{1.75}Y_{0.25}O_3$ corresponds to 380 K at this composition to estimate the order-disorder transition temperature in following section. The energies of the SQSs are not same, even in the same type of SQS. One of the reasons why the energies are not same is the difference of correlation functions from that of the disordered structure. The difference of correlation functions, $\varphi_\alpha - \varphi_\alpha(\mathrm{disorder})$ were shown in Table 1. In the ideal SQSs which mimic a disordered structure perfectly, all of these values should be zero. However, the selected SQSs still have positive or negative values and they reflected the difference of the energies. Then, the energy range of 25 mol% is larger compared to that of 12.5 mol%. This is considered because the difference of energy dependence of oxygen configuration between pure Bi_2O_3 and Y_2O_3. The Y_2O_3 has larger energy range against oxygen configurations than Bi_2O_3 by calculation of many oxygen configurations in a defective fluorite structure [27].

In Y_2O_3 25 mol% system, the energies of SQS-S.A.s are much closer than that of others. The SQS-S.A.s have many $\varphi_\alpha - \varphi_\alpha(\mathrm{disorder})$ of 0 as shown in Table 2, which means that these structures mimic a perfectly disordered structure well and the error between SQS-S.A.s should be small. This is considered to be the reason the energies of SQS-S.A.s well converged. This was not observed in Y_2O_3 12.5 mol% system. If we consider within 20 atoms of δ-Bi_2O_3-M_2O_3, there are eight cations. When we considered the configuration of 12.5 mol%, eight atoms are needed at least. However, in the case of 25 mol%, the smallest number of atoms could be four and it may be easier to take ideal value of the correlation function than 12.5 mol% by search within eight atoms. This may be one of the reasons why SQS-S.A. of 25 mol% can mimic a perfectly disordered structure well. The SQSs at the concentrations of 25, 50, and 75 mol% can similarly mimic a perfectly disordered structure better than other concentrations. This means that the error of estimated energy depends on concentration if SQSs is used. Analogic problems occurred in special structures search to estimate the energy of ordered structure in following section.

In following section, the energy of the disordered structure was evaluated by averaging the energies of random structures. The energy is obtained by averaging the energies of 20 random configurations of cation and oxygen ion with 2×2×2 supercell of the fluorite unit cell.

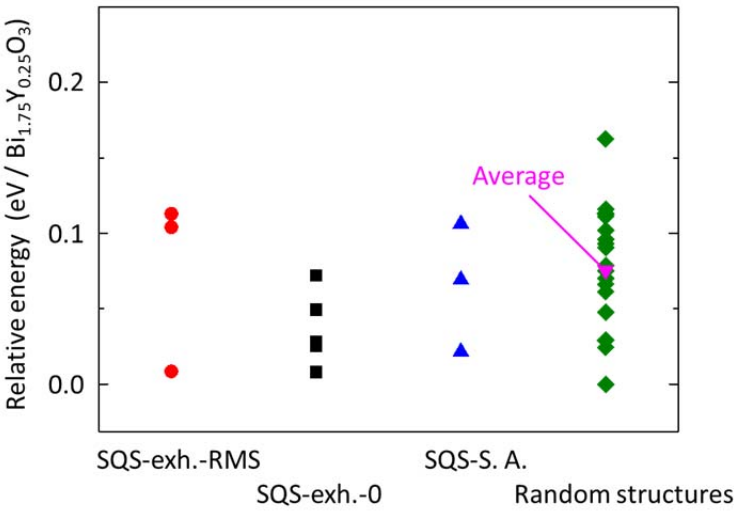

Figure 5. Relative energies in 12.5 mol% Y_2O_3 system

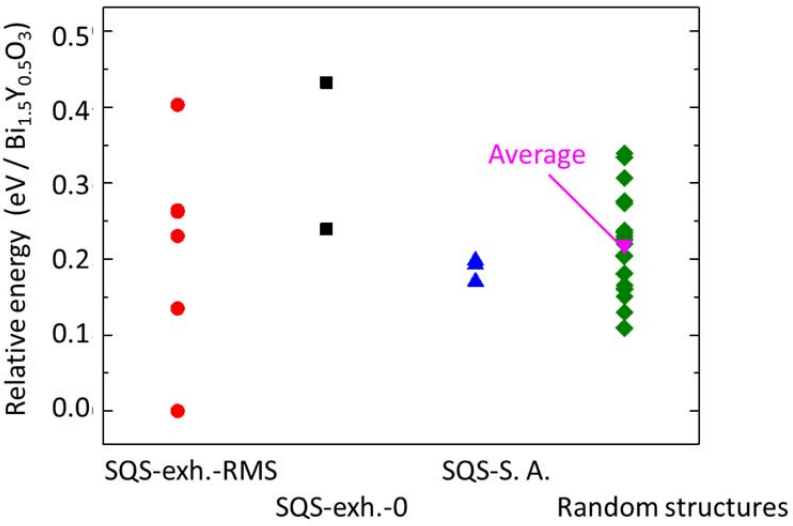

Figure 6. Relative energies in 25 mol% Y_2O_3 system

4. Exploration of ordered structures

To estimate the energy of the ordered structure for each composition, the most stable structure should be determined from a considerable number of candidate structures. Table 3 shows the number of all symmetrically independent configurations for each composition of Bi_2O_3-M_2O_3 system within 20 atoms. Although the configurations are enumerated within 20 atoms, the number of configurations becomes much larger considering a larger supercell. The total number of configurations within 20 atoms is 327460; hence it is prohibitive to compute the energies of all the configurations directly by the DFT calculation.

Generally, the cluster expansion method is useful for searching the ground state ordered structure and estimating the energy of the disordered structure. The δ-Bi_2O_3 solution systems are, however, not better suited for the cluster expansion method because of difficulty to obtain enough accuracy derived from the substantial relaxation of its oxygen positions. Thus, we propose the efficient method based on the cluster expansion method.

Alternately, we explore the stable ordered structures only by calculating the DFT energies of a small number of structures selected by the analysis of the correlation functions used in the CE method. In the CE method, the configurational energy E of a binary system is expressed as eq. (2), $E = \sum_\alpha V_\alpha \varphi_\alpha$. A set of the correlation functions describes the atomic configuration. Hart proposed a hypothesis that the structure with the minimum or maximum energies are involved in structures having high relative likelihood index, based on the inspection of the existing structures in the binary intermetallic compounds [22]. This hypothesis was successfully applied to predict the energy of the most stable structure in a more complicated system such as LISICON-type materials [23]. In this work, the relative likelihood index Φ is defined by the root mean squared difference between the correlation functions of a candidate structure and those of the purely disordered structure, $\varphi_\alpha(\mathrm{disorder})$, as

$$\Phi = \sqrt{\frac{1}{n}\sum_\alpha \{\varphi_\alpha - \varphi_\alpha(\mathrm{disorder})\}^2}, \qquad (4)$$

where n means the number of clusters. The correlation functions of the perfectly disordered structure can be analytically obtained according to its composition. Here, we

hereafter call the structures with a high relative likelihood index “special structures”.

The special structures belong to a group of minority structures as shown in Figure 7, a schema of a distribution function of the structure population in the space of correlation functions. As shown in this schema, the peak of the structure population corresponds to the purely disordered structure. On the other hand, the number of structures with high relative likelihood index, i.e., special structures is much smaller than that of structures near the purely disordered structure. This means that most of possible configurations are not needed to find the most stable structure. By considering only a small number of special structures, the most stable structure is expected to find.

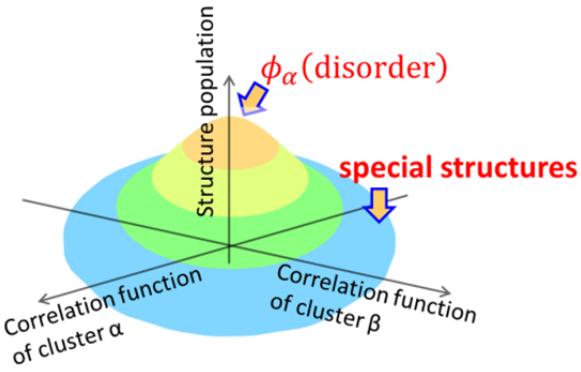

Figure 7. Schematic illustration of structure population in two dimensional correlation function space. The structure group near the outer edge, whose number is small, is defined as special structures.

We consider all configurations of the 2×1×1 fluorite unit cell and all configurations within 20 atoms. The former is for the demonstration of predictive power of special structures in pure Bi_2O_3 and the latter is for finding the most stable structures in Bi_2O_3-M_2O_3 systems. Subsequently, special structures were selected from all the configurations in each case. To calculate the relative likelihood index Φ, we must decide to use which clusters. We considered only pair clusters to calculate Φ. There are three types of pair interactions; anion-anion, anion-cation, and cation-cation. We considered all of them up to the distance of 7 Å, which includes seventh nearest neighbor anion-anion, third nearest anion-cation, and third nearest cation-cation pairs. The enumeration of possible configurations and calculation of their correlation functions are performed by the CLUPAN code [26]. The number of the selected special structures and all possible configurations within 20 atoms are shown in Table 3. Both the configurations of cation and oxygen ion are included, while only the configuration of oxygen ions is considered in the end members. As listed in Table 3, a small number of the special structures are selected compared to a large number of all configurations.

Table 3. The number of special structures and all independent configurations in Bi_2O_3-M_2O_3 system

Composition	**The number of special structures**	**The number of all configurations**
Bi_2O_3, M_2O_3	93	1695
$(Bi_{1/8}M_{7/8})_2O_3$, $(Bi_{7/8}M_{1/8})_2O_3$	98	10391
$(Bi_{2/8}M_{6/8})_2O_3$, $(Bi_{6/8}M_{2/8})_2O_3$	156	35979
$(Bi_{3/8}M_{5/8})_2O_3$, $(Bi_{5/8}M_{3/8})_2O_3$	206	70167
$(Bi_{4/8}M_{4/8})_2O_3$	241	90996
Bi_2O_3-M_2O_3	1357	327460

Then, we carried out the DFT calculation for the special structures. Supercells for the DFT calculation were made by expanding to 80 atoms. The 2×1×1 supercell of the special structures was expanded to 2×2×2 supercell with keeping the atomic configuration. The supercell within 20 atoms was expanded to 80 atoms supercell by multiplying each axis by integer numbers to make near cubic shape with keeping the atomic configuration of the special structures. To remove all symmetry constraints, all atoms in the expanded supercell were displaced randomly within 0.1 Å. DFT calculations were performed by projector augmented-wave (PAW) method [28,29] implemented in the VASP code [30,31]. The radii of the PAW potentials were 1.6 Å for Bi, 1.8 Å for Y, 1.5 Å for La, 1.6 Å for lanthanoid elements other than La, and 0.9 Å for O. The exchange-correlation term was treated with the Perdew-Burke-Ernzerhof functional [32]. The plane-wave cutoff energies were set to be 300 eV. The integration in the reciprocal space is performed at the Γ-point only.

Firstly, we compared the internal energies of special structures with those of all possible configurations in pure Bi_2O_3 to demonstrate the predictive power of the special structures search. Figure 8 shows the energies of special structures and all possible configurations in pure Bi_2O_3 of 2×1×1 expansion of the fluorite unit cell shown in Figure 2. There are 57 symmetrically independent configurations and we selected seven structures as special structures. The origin of the energy is set to the energy of the most stable structure. As can be seen in Figure 8, the structures with maximum and minimum energies are included in special structures. This result suggests that the energy of the ground state ordered structure can be obtained by the calculations only for special structures.

Figure 9 shows Φ dependence of the energies, in which the Φ was calculated up to 1st, 3rd, and 5th nearest neighbors. When we take only 1st nearest neighbor, the variation of the value Φ is only three, 0.00, 0.25, and 0.75. Although the most stable structure was obtained by the structures with the second largest Φ, the number of the structure to calculate is too large. The same problem occurred in the case of Φ up to 3rd nearest neighbors. On the other hand, using Φ up to 5th nearest neighbors, there are only seven structures with the largest and second largest Φ and the most stable structure can be obtained by calculation of the small number of structures.

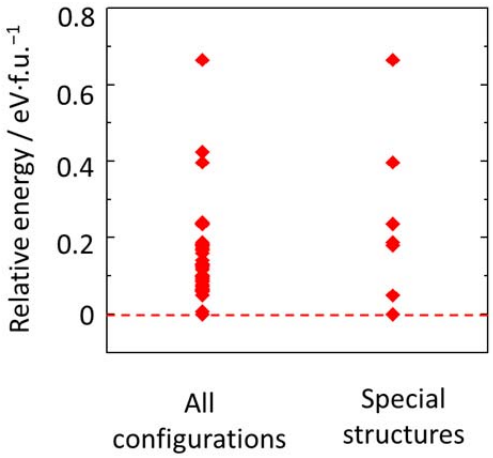

Figure 8. Relative energies of special structures and all configurations. The structures with maximum and minimum energies are included in special structures.

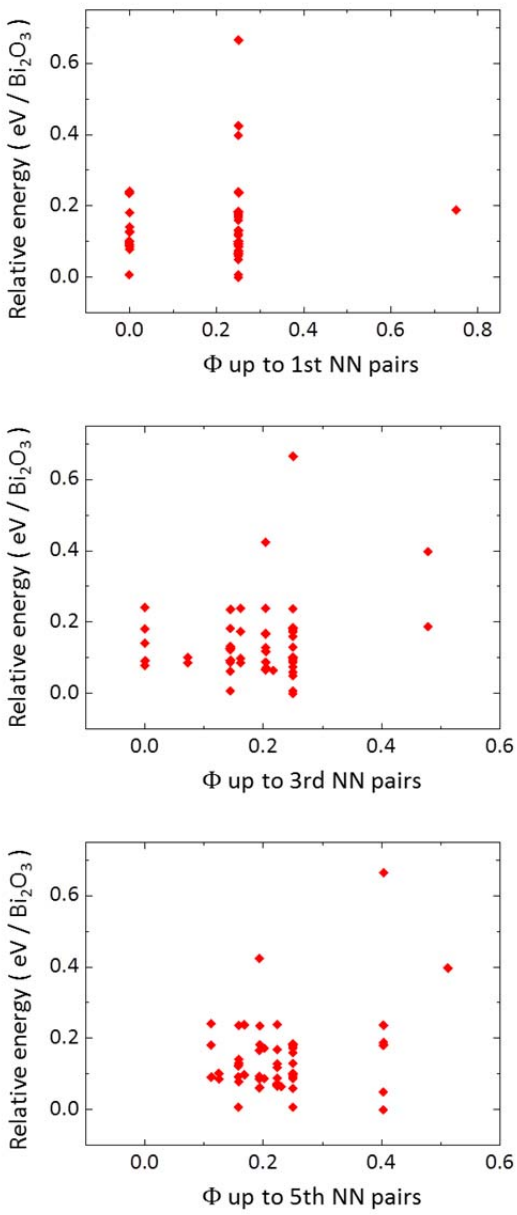

Figure 9. Φ dependence of the energies of special structures

Then, the energies of special structures of Bi_2O_3-M_2O_3 system are calculated. The composition of M_2O_3 ranges from 0 to 1 at the interval of 1/8. To estimate the most stable structures of all Bi_2O_3-M_2O_3 systems, the total number of the DFT structures to estimate the most stable structures of all Bi_2O_3-M_2O_3 systems was 10949. Figure 10 shows formation energies of the most stable structures in Bi_2O_3-M_2O_3 systems by special structures calculations. We could find zig-zag bend against concentration and this bend was found in Bi_2O_3-M_2O_3 systems. The energies of 12.5, 37.5, 62.5, and 87.5 mol% are relatively high in these zig-zag bends. When the special structure searched in this work, the atom numbers within 20 were considered and this included eight cations. When we considered those concentrations, 12.5, 37.5, 62.5, and 87.5 mol%, the 8 atoms are needed at least to express the atom configuration. In this case, it is difficult to take the ideal values of φ_α about many species of cluster α as shown in special quasirandom structures to estimate the energy of disordered structure as described in the section before. On the other hand, less 25, 50, and 75 mol% can be expressed by number of cations configurations. For example, 50 mol% can be expressed by two, four, six, and eight atoms. This implies that more enough searching of special structures can be performed and high possibility of finding more stable structure. Similar problem also occurred and discussed in SQSs to estimate the energy of disordered structure as described in the section before.

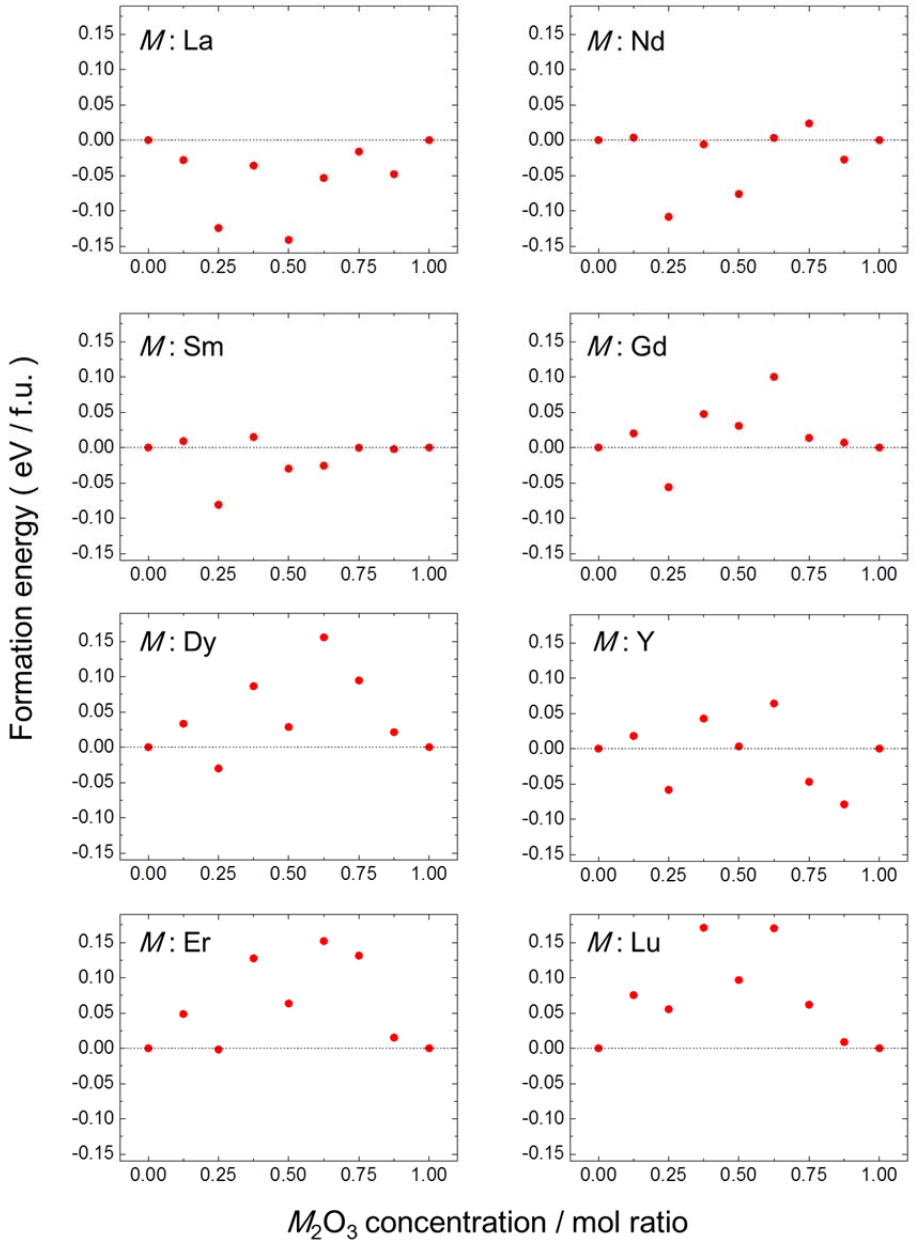

Figure 10. Formation energies of most stable structures in Bi_2O_3-M_2O_3 systems by special structures calculations

5. Estimation of the order-disorder transition temperature

Once the most stable structures are explored and their energies are calculated, the order-disorder transition temperature T_c is approximately estimated from the energy difference between the ordered and purely disordered structures. The configurational entropy effect is considered only for the disordered structure. In this approximation, the order-disorder transition temperature T_c is derived from the free energy relationship, expressed as $E_{\mathrm{order}} = E_{\mathrm{disorder}} - T_c S_{\mathrm{disorder}}$ where E_{order}, E_{disorder} and S_{disorder} denote the energy of the ordered structure, the energy of the purely disordered structures and the configurational entropy of the purely disordered structure, respectively. The entropy for the purely disordered structure is simply estimated by the point approximation expressed by

$$S_{\mathrm{disorder}} = k \ln W \cong -kn\{x \ln x + (1-x)\ln(1-x)\}, \qquad (5)$$

where k means Boltzmann constant, W means the number of configurations, n means the number of sites and x means concentration of anion or cation.

Firstly, we estimated the order-disorder transition temperature of pure Bi_2O_3. The order-disorder transition temperature was predicted to be 1070 K. This is close to the β-δ transition temperature of around 900 K although simple approximations for the free energy of the purely disordered structure are used. This phase transition can be regarded as the order-disorder transition because the β phase is tetragonal and can be assumed as a distorted and ordered δ phase where the oxygen vacancies were arranged along the [100] direction [3,5,33,34].

Then, we evaluate the order-disorder transition temperatures in Bi_2O_3-M_2O_3 systems. Figure 11(a) shows predicted T_c in Bi_2O_3-M_2O_3 systems. The predicted T_c at high solutes concentrations, 87.5 and 100 mol% was very high compared to that of other concentrations. This is consistent with the fact that M_2O_3 is stable at high temperature as C-type rare-earth structure, which can be assumed as ordered phase in this work. Figure 11(b) shows concentration dependence of the predicted T_c in the Bi_2O_3-Er_2O_3 system. The predicted T_c became high in the region of high Er_2O_3 concentration. The square dots mean the results of reported experiments. The square on Bi_2O_3 means the β-δ transition temperature of pure Bi_2O_3 as described before. The squares in the region of solution of Bi_2O_3 and Er_2O_3 mean the deflection of ionic

conductivity at each composition [14]. Er_2O_3 is stable as C-type rare-earth structure, which can be considered as ordered δ phase in this work, up to 2300 K and has transition to hexagonal phase occurred at this temperature as the square dot at Er_2O_3 [35,36]. Our result of higher T_c of Er_2O_3 than this transition temperature is consistent because the order-disorder transition should occur at higher temperature than the transition temperature between the C-type rare earth structure and the hexagonal phase. As shown in Figure 11(b), the predicted T_c in the Bi_2O_3-Er_2O_3 system is consistent with previous experimental reports and the prediction of T_c agrees with experiments in the other rare-earth alloyed Bi_2O_3, as well. These results imply that the deflection of ionic conductivity of rare-earth-alloyed Bi_2O_3 is due to order-disorder transition of oxygen sublattice. Figure 11(c) shows the predicted T_c at 25 mol% solutes concentration as a function of solutes' ionic radius. Experimental data of the deflection point of ionic conductivity was plotted [14,15,37] and they reveal good agreements with predicted T_c.

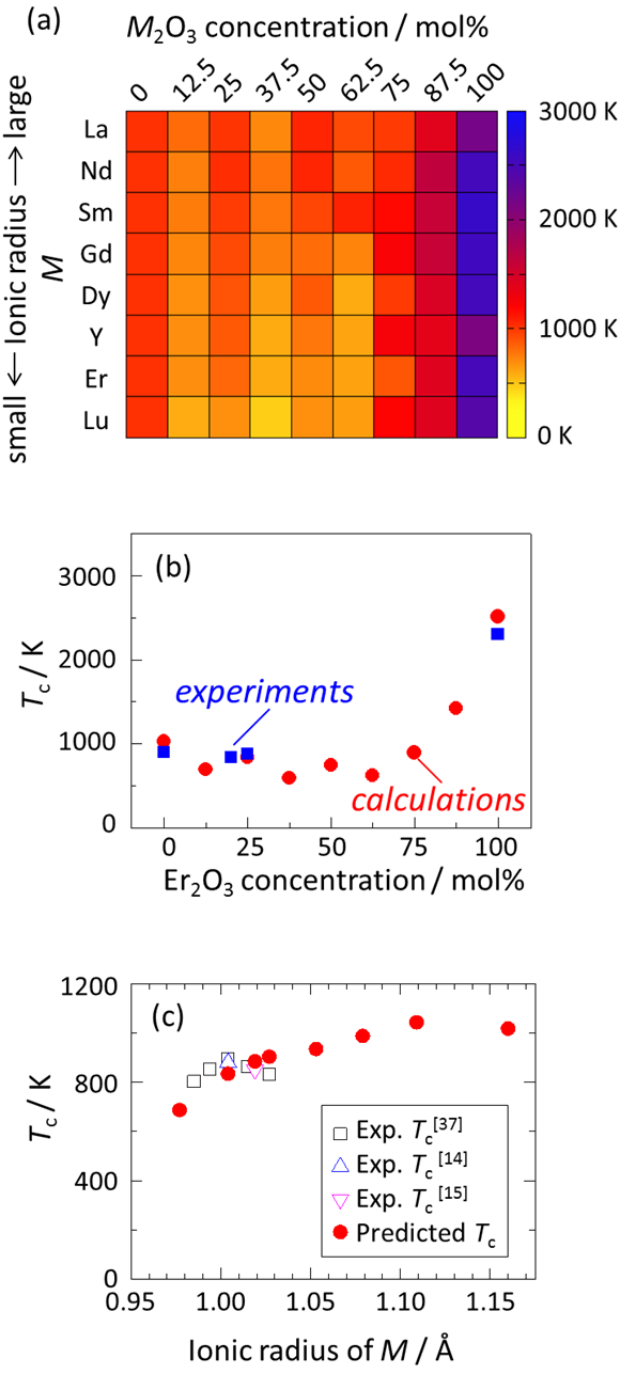

Figure 11. (a) The predicted T_c in δ-Bi_2O_3-M_2O_3 systems (b) Comparison between the predicted T_c and experimental T_c in δ-Bi_2O_3-Er_2O_3 system (c) Comparison between the predicted T_c and experimental deflection temperature of ionic conductivity at M concentration of 25 mol%.

6. Summary

In order to obtain the knowledge about the deflection of ionic conductivity, we predicted the order-disorder transition temperature in δ-Bi_2O_3-M_2O_3 system, considering that the deflection is due to the order-disorder transition of oxide ion. The order-disorder transition temperature T_c was predicted by estimating the free energies of order and disordered structures. We propose the special structures search to estimate the ground state ordered structure's energy efficiently.

The predictive potential of the special structures search was demonstrated in pure δ-Bi_2O_3. The ground state ordered structure can be obtained by calculation only for special structures. The predicted T_c was consistent with the experimental β-δ transition temperature, which can be assumed as the oxygen order-disorder transition in this work. The predicted T_c in δ-Bi_2O_3-M_2O_3 system represents good agreement with the deflection temperature of ionic conductivity. This result implies that the deflection of ionic conductivity is due to order-disorder transition of oxygen sublattice. Our method can reduced the number of calculation structures drastically and it is easy to apply other many systems involved in order-disorder transition.

References

[1] P. Knauth and H. Tuller, J. Am. Ceram. Soc. **80**, 1654 (2002).

[2] A. M. Azad, S. Larose, and S. A. Akbar, J. Mater. Sci. **29**, 4135 (1994).

[3] H. A. Harwig and A. G. Gerards, Thermochim. Acta **28**, 121 (1979).

[4] T. Takahashi and H. Iwahara, Mater. Res. Bull. **13**, 1447 (1978).

[5] G. Gattow and D. Schütze, Zeitschrift Für Anorg. Und … **546**, (1964).

[6] P. D. Battle and C. R. A. Catlow, J. Phys. C: Solid State Phys. **16**, L561 (1983).

[7] M. Yashima and D. Ishimura, Chem. Phys. Lett. **378**, 395 (2003).

[8] C. Mohn, S. Stølen, S. Norberg, and S. Hull, Phys. Rev. Lett. **102**, 100 (2009).

[9] S. Hull, S. T. Norberg, M. G. Tucker, S. G. Eriksson, C. E. Mohn, and S. Stølen, Dalton Trans. 8737 (2009).

[10] A. Seko, Y. Koyama, A. Matsumoto, and I. Tanaka, J. Phys. Condens. Matter **24**, 475402 (2012).

[11] C. Mohn, S. Stølen, S. Norberg, and S. Hull, Phys. Rev. B **80**, 1 (2009).

[12] P. Shuk, H. D. Wiemhöfer, U. Guth, W. Göpel, and M. Greenblatt, Solid State Ionics **89**, 179 (1996).

[13] N. Sammes, G. Tompsett, H. Nafe, and F. Aldinger, J. Eur. Ceram. Soc. **19**, (1999).

[14] M. Verkerk and K. Keizer, J. Appl. Electrochem. **10**, (1980).

[15] T. Takahashi, H. Iwahara, and T. Arao, J. Appl. Electrochem. **5**, 187 (1975).

[16] T. Takahashi, T. Esaka, and H. Iwahara, J. Appl. Electrochem. **5**, 197 (1975).

[17] P. Hohenberg and W. Kohn, Phys. Rev. **155**, (1964).

[18] W. Kohn and L. Sham, Phys. Rev. **385**, (1965).

[19] J. Sanchez, F. Ducastelle, and D. Gratias, Phys. A Stat. Mech. … 334 (1984).

[20] D. Fontaine, Solid State Phys. **47**, 33 (1994).

[21] F. Ducastelle, *Order and Phase Stability in Alloys* (Elsevier, New York, 1992).

[22] G. L. W. Hart, Nat. Mater. **6**, 941 (2007).

[23] K. Fujimura, A. Seko, Y. Koyama, A. Kuwabara, I. Kishida, K. Shitara, C. A. J. Fisher, H. Moriwake, and I. Tanaka, Adv. Energy Mater. **3**, 980 (2013).

[24] K. Momma and F. Izumi, J. Appl. Crystallogr. **41**, 653 (2008).

[25] A. Zunger, S. Wei, L. Ferreira, and J. Bernard, Phys. Rev. Lett. **65**, 353 (1990).

[26] A. Seko, Y. Koyama, and I. Tanaka, Phys. Rev. B **80**, 1 (2009).

[27] A. Matsumoto, K. Yuge, Y. Koyama, and I. Tanaka, in *Jt. Symp. Mater. Sci. Eng. 21st Century* (Hsinch, Taiwan, 2007).

[28] P. Blöchl, Phys. Rev. B **50**, (1994).

[29] G. Kresse and D. Joubert, Phys. Rev. B **59**, 11 (1999).

[30] G. Kresse and J. Hafner, Phys. Rev. B **47**, (1993).

[31] G. Kresse and J. Furthmüller, Comput. Mater. Sci. **6**, 15 (1996).

[32] J. Perdew, K. Burke, and M. Ernzerhof, Phys. Rev. Lett. **77**, 3865 (1996).

[33] C. Rao, G. Rao, and S. Ramdas, J. Phys. Chem. **45**, 672 (1969).

[34] A. Matsumoto, Y. Koyama, and I. Tanaka, Phys. Rev. B **81**, 1 (2010).

[35] Z. Heiba, H. Okuyucu, and Y. S. Hascicek, J. Appl. Crystallogr. **35**, 577 (2002).

[36] A. Ginya and I. Nobuhito, Chem. Rev. **98**, 1479 (1998).

[37] H. T. Cahen, T. G. M. Van Den Belt, J. H. W. De Wit, and G. H. J. Broers, Solid State Ionics **1**, 411 (1980).

Chapter 3

Analysis of Ionic Conductivity of Bi_2O_3 and Rare-earth Oxides Solution by Systematic First-principles Molecular Dynamics

1. Introduction

Oxide ionic conductors have been used as oxygen sensors, solid oxide fuel cells and oxygen separation membranes [1,2]. Bismuth sesquioxide with a cubic form, δ-Bi_2O_3, is one of oxide materials with a high oxide ionic conductivity. The δ-Bi_2O_3 shows oxygen conductivity of nearly 1 S/cm at high temperatures better than that of yttria stabilized zirconia (YSZ) [3,4]. This high ionic conductivity has been revealed to originate from the crystal structure of the δ-Bi_2O_3. The δ-Bi_2O_3 has a defective fluorite structure, where empty oxygen sites are distributed randomly for the charge neutrality [5–10]. The disordering on the oxygen sublattice is related to its high ionic conductivity, which is examined by first-principles molecular dynamics simulations [10,11]. However, the δ phase is stable only in the temperature range between 1002 K and melting point of 1097 K. The phase transition was reported from δ phase to other phases, α, β, and γ, depending on cooling rates and these phases reveal a drastic decrease of the oxygen conductivity [3,12].

The reported δ-Bi_2O_3 is shown in Figure 1 [7]. The δ-Bi_2O_3 has the defective fluorite structure, cation forms face-centered cubic (fcc) and oxygen was placed on the center of cations tetrahedron. A quarter of oxygen is empty and oxygen atoms are disordered. The total oxygen occupancy is 3/4. Oxygen occupies not only the 8c but also the 32f sites and diffuses <100> direction to the next 8c sites through the 32f sites. Pure δ-Bi_2O_3 has been well investigated by analysis of powder neutron diffraction data and first-principles calculations. M. Yashima reported that oxygen is expanded to 32f

sites from 8c sites and diffuses along <100> direction by analysis of powder neutron diffraction data by maximum entropy method [7]. C.E. Mohn and A. Seko also reported the expansion to 32f sites of oxygen by first-principles molecular dynamics (MD) [10,11].

The use of a solid solution of Bi_2O_3 and some rare-earth oxides has been known as one of the methods to stabilize the δ phase at room temperature [13]. For instance, an yttrium oxide stabilized δ-Bi_2O_3, especially Y_2O_3 25 mol% doped Bi_2O_3 among them, shows a high ionic conductivity comparable to that of pure δ-Bi_2O_3 at high temperatures as shown in Figure 2 [14]. However, the conductivity is lower with the increase of the solute concentration. This tendency is observed also in other solutes, Er, Dy, and Gd [15–17]. There are few reports about oxygen diffusion mechanism of a solid solution of Bi_2O_3 and some rare-earth oxides. M. Yashima reported the structure of the ytterbium substituted system $Bi_{1.4}Yb_{0.6}O_3$ [18]. In this report, the cation sublattice is also disordered. M. Krynski reported that yttrium traps oxygen and disrupts oxygen diffusions in δ-Bi_3YO_6 by first-principles MD [19].

The effects on the ionic conductivity of alloying with rare-earth elements are not clearly revealed for various rare-earth elements. In order to investigate the origin of the decrease of ionic conductivity, it is considered to be useful to construct and analyze the systematic database of ionic conductivity. Lately, the databases about materials have been constructed by first-principles calculation, for example Materials Project and Aflowlib [20,21]. However, they are not plenum about the properties like ionic conductivity which is expensive in the view point of calculation costs and most of their data is about reported structure in International Crystal Structure Database. Those properties of not reported composition or structure need to be calculated. Although the exhaustive database about ionic conductivity can be constructed by the first-principles MD, however, it is hardly cheap to calculate exhaustive systems. In addition, it is useful to predict the conductivity of other systems without molecular dynamics from the systematic database. For these purposes, the analyses of information science will be helpful. There are two purposes of using the information science technology. One is a discovery of the relationship we have never found. The other is the prediction of ionic conductivity without experiments or heavy calculations.

In this work, first-principles MD simulations of eight kinds of Bi_2O_3-M_2O_3

systems (*M*=La, Nd, Sm, Gd, Dy, Y, Er, Lu) were performed at several temperatures for investigation of the effect on the ionic conductivity of alloying with rare-earth elements. After molecular dynamics simulations, self-diffusion coefficients and two types of distribution functions, angular and radial, were calculated. Temperature and composition dependence of them and relationship between them were investigated. Furthermore, the systematic database of ionic conductivity was constructed the informatics analyses were performed to find the relationship between some parameters and predict the material property, diffusion coefficients.

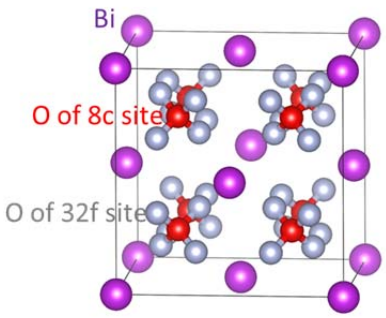

Figure 1. Structure of pure δ-Bi_2O_3. This figure was drown by VESTA code [22].

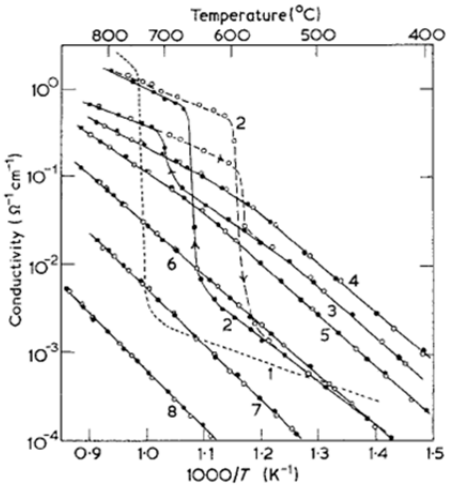

Figure 2. Reported conductivity in $(Bi_2O_3)_{1-x}(Y_2O_3)_x$ [14]. The values for *x* are: 1-0; 2-0.05; 3-0.20; 4-0.25; 5-0.33; 6-0.425; 7-0.50; 8-0.60.

2 Method

2-1. First-principles molecular dynamics

We performed systematic first-principles MD calculations in eight kinds of Bi_2O_3-M_2O_3 systems (M=La, Nd, Sm, Gd, Dy, Y, Er, Lu). The composition of M_2O_3 ranges from 0 to 1 at the interval of 1/8. The initial structures were needed before MD calculations. As described before, the δ-Bi_2O_3 has the fluorite structure, where cation forms face-centered cubic (fcc) and oxygen was placed on the center of cations tetrahedron. The total oxygen occupancy is 3/4 because a quarter of oxygen is empty and oxygen atoms are disordered. Although it is suggested that not only the 8c but also the 32f sites are occupied by oxygen atoms in δ-Bi_2O_3, the configurations of oxygen atoms on the 32f sites are not considered as initial structures, shown in Figure 3. The cation sites in δ-Bi_2O_3-M_2O_3 systems are set as also disordered based on the previous experimental reports by analysis of powder neutron diffraction [18,23]. The cell volumes of initial structures were determined by averaging the volumes of random structures. Twenty supercells of the 2×2×2 fluorite unit cell were made in which all of cation and oxygen were distributed randomly to each sublattice and structure optimization was performed. Averaging these twenty volumes, the lattice parameters of the fluorite structure in δ-Bi_2O_3-M_2O_3 systems were determined.

The initial atomic configurations were determined by the special quasirandom structures (SQSs) [24]. The supercell size of SQSs was set to 2×2×2 expansion of fluorite unit cell and the SQSs were constructed by CLUPAN code [25] considering nine correlation functions which include up to third nearest neighbor anion-anion pairs, third nearest neighbor cation-cation pairs, and third nearest neighbor anion-cation pairs. The root mean square difference of the correlation functions from that of perfectly disordered structure was used as criteria and simulated annealing was performed.

The first-principles MD simulation was performed within the *NVT* ensemble. The temperature was controlled by the algorithm of Nosé [26,27] and set to three temperatures, 1100, 1600 and 2100 K. The time step was set to 2 fs. The first 1250 steps, i.e. 2.5 ps, are removed from the analysis. Total number of steps was determined by checking convergence of mean square displacement and self-diffusion coefficient. Total

number of steps for analysis is set to 18750 steps, which corresponds to 37.5 ps.

The structure optimization calculations and first-principles MD simulations were performed by the projector augmented-wave (PAW) method [28,29] implemented in the VASP code [30,31]. The radii of the PAW potentials were 1.6 Å for Bi, 1.8 Å for Y, 1.5 Å for La, 1.6 Å for lanthanoid elements other than La, and 0.9 Å for O. The exchange-correlation term was treated with the Perdew-Burke-Ernzerhof functional [32]. The plane-wave cutoff energies were set to be 300 eV. The integration in the reciprocal space is performed at the Γ-point only.

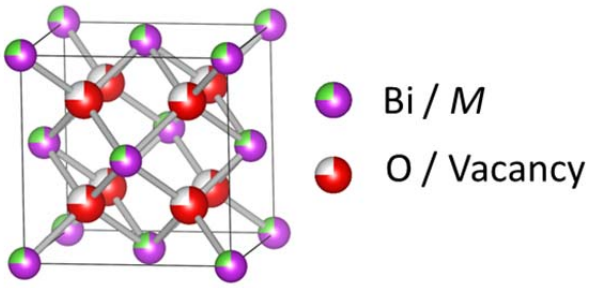

Figure 3. Considered structure of δ-Bi_2O_3-M_2O_3. It has two sublattiaces, cation (bismuth and rare earth element *M*) and anion (oxide ion and vacancy). This figure was drawn by VESTA code [22].

2-2. Analysis and prediction within linear correlation

In order to investigate the results of MD simulations, the database was constructed. The correlation coefficients were calculated and subsequently, some informatics analyses were performed. The performed analyses can be roughly divided into two types, unsupervised learning and supervised learning. The former does not distinguish between target variables and explanatory variables, and the latter distinguishes. Principal component analysis (PCA) was performed as the unsupervised learning and thus, some linear regression methods were performed as the supervised learning [33–35]. The ordinary least-squares regression (OLSR) and the partial least-squares regression (PLSR) [36,37] were performed. Besides the OLSR using all variables, variables are selected by based on Akaike's information criterion regularization (AIC) [38] and "least absolute shrinkage and selection operator" (LASSO) [39]. The variables are normalized to have zero-mean and unit-variance before the analysis and the regressions. The prediction was performed by linear regression methods as well. To estimate the goodness of regression equation, the root mean square error (RMSE) and 5-fold cross validation (CV) score were used. The CV score is to check whether the regression fall into over-fitting or not. Two types of RMSE were considered; one is the RMSE of training dataset, which is used for regression and the other is RMSE of other data which is not used for regression. The former is criteria of the goodness to fit the data. The latter is to check over-fitting and predictive power for extrapolation.

2-2-1. Principal component analysis (PCA)

PCA is classified as an unsupervised learning and used to capture the characteristics of the database. There is no distinction between target and other variables. PCA can be considered as a method to convert original variables which have correlation with each other to new variables "principle component (PC)" which have small correlation with other components by orthogonal rotation. Moreover, it is one of the methods to visualize the two or three dimensional space by projection from multidimensional space with the loss of minimal information. Figure 4 shows an example of PCA in two-dimensional space. Instead of the orthogonal axes of *x* and *y*, new axes *a* and *b* are obtained. The axis *a* is obtained to maximize the variance of data and called as first principle component. The axis *b* is obtained to maximize the variance on the condition to be orthogonal with the axis *a* and called as second principle component.

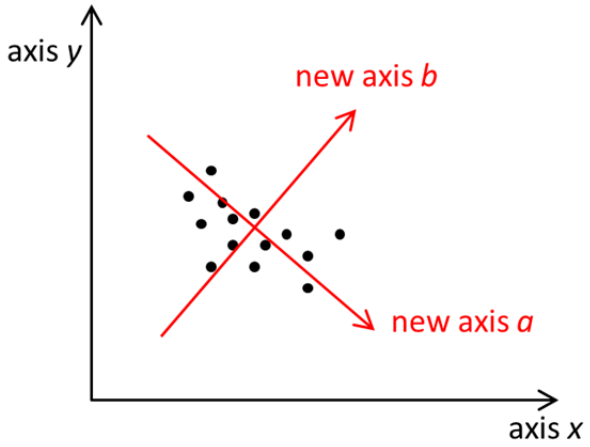

Figure 4. Schematic figure of PCA. The axes *x* and *y* are converted to new axes *a* and *b*, which are called as principles components.

The PCs in the case of multidimensional space, p dimensional space are calculated as followed. Considering n data, $\boldsymbol{x}_1$, $\boldsymbol{x}_2$, …, $\boldsymbol{x}_n$ which have p variables, i.e. $\boldsymbol{x} = (x_1, x_2, \cdots, x_p,)^T$, the Variance-covariance matrix S was calculated as

$$S = (s_{jk}) = \frac{1}{n}\sum_{i=1}^{n}(\boldsymbol{x}_i - \overline{\boldsymbol{x}})(\boldsymbol{x}_i - \overline{\boldsymbol{x}})^T, \quad (1)$$

$$s_{jk} = \frac{1}{n}\sum_{i=1}^{n}(x_{ij} - \bar{x}_j)(x_{ik} - \bar{x}_k), \quad (2)$$

where $\overline{\boldsymbol{x}}$ is p dimensional means vector. The projected new axis y is expressed by linear combination of p variables as

$$y = w_1x_1 + w_2x_2 + \cdots + w_px_p = \boldsymbol{w}^T\boldsymbol{x}, \quad (3)$$

where $\boldsymbol{w}$ is weight vector for new axis y. New one dimensional data, $y_i = \boldsymbol{w}^T\boldsymbol{x_i}$ $(i = 1, 2, \cdots, n)$ are obtained by projection of n data. The mean of this data is expressed as

$$\bar{y} = \frac{1}{n}\sum_{i=1}^{n}\boldsymbol{w}^T\boldsymbol{x_i} = \boldsymbol{w}^T\overline{\boldsymbol{x}}, \quad (4)$$

and the variance of y is expressed as

$$\begin{aligned} {s_y}^2 &= \frac{1}{n}\sum_{i=1}^{n}(y_i - \bar{y})^2 \\ &= \frac{1}{n}\sum_{i=1}^{n}(\boldsymbol{w}^T\boldsymbol{x_i} - \boldsymbol{w}^T\overline{\boldsymbol{x}})^2 \\ &= \boldsymbol{w}^T\frac{1}{n}\sum_{i=1}^{n}(x_i - \bar{x})(x_i - \bar{x})^T\boldsymbol{w} \\ &= \boldsymbol{w}^TS\boldsymbol{w}. \end{aligned} \quad (5)$$

Therefore, the variance and weight vector of y are equal to eigenvalue and eigenvector of the matrix S. Since the first PC is selected to maximize the variance, the largest eigenvalue and its eigenvector are the variance and weight vector of first PC, respectively. The weight vector of second PC is the eigenvector of the second largest eigen value. The weight vector is taken to be length of 1 by standardization and the components of weight vector are called as loading. In general, the criteria to measure the amount of information is given by

$$\frac{\lambda_i}{\lambda_1+\lambda_2+\cdots+\lambda_p}, \quad (6)$$

called as proportion of variance and the amount of information given from first PC to k-th PC is given by

$$\frac{\lambda_1+\lambda_2+\cdots+\lambda_k}{\lambda_1+\lambda_2+\cdots+\lambda_k\cdots+\lambda_p}, \tag{7}$$

called as cumulative proportion.

PCA can compare the importance of variables [40]. The most popular method for this purpose is loading plots, which is visualization of the loading weight $\boldsymbol{w}_i$ in reduced dimension space where i is the number of PC. For example, the value of $\boldsymbol{w}_i$ and $\boldsymbol{w}_j$ are plotted in two dimension space for each original variables. This plot represents whether the variables have linear correlation with other variables or not. The importance of variables for some target variable is represented as the length projected from the variables to the target variable's vector. Therefore, when we consider up to q PCs, the variable importance in the projection of k-th variable is given as

$$\mathrm{VIP}_{\mathrm{PCA},k\text{th variable}} = \frac{\sum_i^q w_i^k w_i^t}{\sum_i^q \sum_r^p w_i^r w_i^t}, \tag{8}$$

where w_i^k is the kth loading weight of i-th PC corresponding to the k-th variable and w_i^t is the target's loading weight of i-th PC corresponding to the target variable.

2-2-2. Ordinary least-squares regression (OLSR)

OLSR is one of the most popular regression methods. This is classified as a supervised learning and it has clear distinction between the target and other variables. Given $\boldsymbol{y}$ as target variable and $\boldsymbol{x}$ as explanatory variable, the regression equation is given as

$$\boldsymbol{y} = \boldsymbol{w}^T\boldsymbol{x} + \boldsymbol{\varepsilon}, \tag{9}$$

where $\boldsymbol{w}$ is regression coefficients and $\boldsymbol{\varepsilon}$ is error. In the OLSR, the regression coefficients are determined by minimizing the mean-squared error for observed data. The minimization function is given as

$$\|\boldsymbol{\varepsilon}\|_2{}^2 = \|\boldsymbol{y} - \boldsymbol{w}^T\boldsymbol{x}\|_2{}^2 = \sum_i^n (y_i - \boldsymbol{w}^T\boldsymbol{x}_i)^2, \tag{10}$$

where $\|\cdot\|_2$ means L_2-norm. However, when the number of predictor variables is large, the regression becomes over-fitting frequently. The dataset is parted into training set and test set performed to confirm whether the regression is over-fitting or not and the variables selection is performed to avoid it. The regression is performed by training dataset and error of test dataset was estimated using the regression equation. As other

method to check over-fitting, the cross validation score is evaluated. There are many methods for variables selection. In this work, two methods are applied. One is a stepwise regression method with bidirectional elimination [41] based on minimization of the Akaike's information criterion (AIC). The other is least absolute shrinkage and selection operator (LASSO).

AIC is defined as

$$\mathrm{AIC} = -2\ln(L) + 2k, \tag{11}$$

where L is the maximum likelihood of the constructed model and k is the number of variables. In the linear regression model where the normal distribution is assumed, the AIC is given as

$$\mathrm{AIC} = n \times \ln\left(\frac{\|\boldsymbol{y}-\boldsymbol{w}^T\boldsymbol{x}\|_2{}^2}{n}\right) + 2k, \tag{12}$$

where n is the number of data. In this work, this equation was used.

2-2-3. Least Absolute Shrinkage and Selection Operator (LASSO)

The difference between OLSR using all variables and LASSO is the minimization function. The minimization function is given as

$$\begin{aligned} L &= \|\boldsymbol{y} - \boldsymbol{w}^T\boldsymbol{x}\|_2{}^2 + \lambda\|\boldsymbol{w}\|_1 \\ &= \|\boldsymbol{y} - \boldsymbol{w}^T\boldsymbol{x}\|_2{}^2 + \lambda\sum_j|w_j|, \end{aligned} \tag{13}$$

where the second term is called as regularization term which controls complexity of the regression equation. λ in the second term is regularization coefficient which controls the trade-off relationship between the sparsity and accuracy for training data of the regression equation. In LASSO regression, the many of coefficients w_j becomes zero because of L_1-norm, $\sum_j|w_j|$ and the variable selection is performed automatically.

2-2-4. Partial least-squares regression (PLSR)

PLSR is used when the variables have multicolinearlity and it combines features of OLSR and PCA. PCA finds the combination of variables by variance of data and reduces the multicolinearlity between new variables, principle components. Although these PCs consider the relationship with the target variable, however, there is

no guarantee of contribution for regression of the target variable. In order to resolve this problem, PLSR finds the combination of variables by the variance between target and principles components. Although there are many algorithms for determination of new variables, the non-linear iterative partial least square (NIPALS) algorithm was used in this study [36]. It does not calculate all the principle components at once. Assume that the $n \times p$ matrix $\boldsymbol{X}$ and the column vector $\boldsymbol{y}$ have been standardized to have mean zero and unit variance. In case of PLSR with a single response variable, the PLSR model with h ($h \leq p$) latent variables can be expressed as follows.

$$\boldsymbol{X} = \boldsymbol{T}\boldsymbol{P}^{t} + \boldsymbol{E}, \tag{14}$$

$$\boldsymbol{y} = \boldsymbol{T}\boldsymbol{b} + \boldsymbol{f}, \tag{15}$$

where $\boldsymbol{X}(n \times p)$, $\boldsymbol{T}(n \times h)$, $\boldsymbol{P}(p \times h)$, $\boldsymbol{y}(n \times 1)$, and $\boldsymbol{b}(h \times 1)$ are respectively used for predictors, $\boldsymbol{X}$ scores, $\boldsymbol{X}$ loadings, a response and regression coefficients of $\boldsymbol{T}$. $\boldsymbol{E}$ and $\boldsymbol{f}$ are residuals if we take h latent variables. Generally, a weight matrix $\boldsymbol{W}(p \times h)$ is obtained to make $\|\boldsymbol{f}\|$ as small as possible to derive a useful relation between $\boldsymbol{X}$ and $\boldsymbol{y}$ by using NIPALS algorithm. The NIPALS algorithm is follows:

Input: $\boldsymbol{E}_0=\boldsymbol{X}$, $\boldsymbol{f}_0=\boldsymbol{y}$

Output: $\boldsymbol{W}$, $\boldsymbol{b}$, $\boldsymbol{T}$, $\boldsymbol{P}$

for all $k = 1,\ldots,h$ do

step 1 : $\boldsymbol{w}_k = \boldsymbol{E}_{k-1}^{\mathrm{T}}\boldsymbol{f}_{k-1}/\| \boldsymbol{E}_{k-1}^{\mathrm{T}}\boldsymbol{f}_{k-1}\|$

step 2 : $\boldsymbol{t}_k = \boldsymbol{E}_{k-1}\boldsymbol{w}_k/(\boldsymbol{w}_k^{\mathrm{T}}\boldsymbol{w}_k)$

step 3 : $b_k = \boldsymbol{f}_{k-1}^{\mathrm{T}}\boldsymbol{t}_k/(\boldsymbol{t}_k^{\mathrm{T}}\boldsymbol{t}_k)$

step 4 : $\boldsymbol{p}_k = \boldsymbol{E}_{k-1}^{\mathrm{T}}\boldsymbol{t}_k/(\boldsymbol{t}_k^{\mathrm{T}}\boldsymbol{t}_k)$

step 5 : $\boldsymbol{E}_{\mathrm{k}} = \boldsymbol{E}_{k-1} - \boldsymbol{t}_k\boldsymbol{p}_k^{\mathrm{T}}$

step 6 : $\boldsymbol{f}_k = \boldsymbol{f}_{k-1} - b_k\boldsymbol{t}_k$

end for

---

where $\boldsymbol{p}_k$ and b_k are the hth components of $\boldsymbol{P}$ and $\boldsymbol{b}$, respectively. Using weight matrix $\boldsymbol{W}$ obtained by NIPALS algorithm, the regression model can be written as

$$\boldsymbol{y} = \boldsymbol{X}\boldsymbol{W}^{*}\boldsymbol{b} = \boldsymbol{X}\boldsymbol{b}_{\mathrm{pls}}, \tag{16}$$

where $\boldsymbol{W}^{*}$ satisfies the equation $\boldsymbol{W}^{*} = \boldsymbol{W}(\boldsymbol{P}^{\mathrm{T}}\boldsymbol{W})^{-1}$. Therefore, the coefficients of the

linear regression with original variables can be obtained as $\boldsymbol{b}_{\text{pls}}$ equal to $\boldsymbol{W}^{*}\boldsymbol{b}$.

Moreover, VIP in PLSR, VIP_{PLSR} is calculated, which is a summary of the importance for the projection to find h latent variables [37]. The VIP_{PLS} for the j-th variable is written as

$$\text{VIP}_{\text{PLSR},j} = \sqrt{p \sum_{k=1}^{h} \left(SS(b_k \boldsymbol{t}_k) \left(w_{jk} / \|\boldsymbol{w}_k\| \right)^2 \right) / \sum_{k=1}^{h} SS(b_k \boldsymbol{t}_k)}, \qquad (17)$$

where $SS(b_k \boldsymbol{t}_k) = {b_k}^2 {\boldsymbol{t}_k}^T \boldsymbol{t}_k$. Since the mean of squared VIP_{PLSR} scores equals 1, the variable with greater VIP_{PLSR} than 1 can be considered as important or contributory to the regression.

3. Results and discussions

3-1. First-principles molecular dynamics

3-1-1. Diffusion coefficients and ionic conductivity

The self-diffusion coefficients of the atoms can be estimated by the trajectory of the atoms obtained from first-principles MD simulations. According to the Einstein relation, the self-diffusion coefficient is given by

$$D_\xi = \lim_{t\to\infty} \frac{\langle r^2\rangle_\xi}{6t}, \tag{18}$$

where $\langle r^2\rangle_\xi$ denotes the mean square displacement (MSD) of atom ξ, and t is the simulation time. The MSD of atom ξ, $\langle r^2\rangle_\xi$ is given by

$$\langle r^2\rangle_\xi = \frac{1}{N_\xi}\sum_i \left(\overrightarrow{r_i(t)} - \overrightarrow{r_i(0)}\right)^2, \tag{19}$$

where N_ξ is the number of atom ξ in the simulation cell and $\overrightarrow{r_i(t)}$ is the position of atom i at time t.

Figure 5(a) shows the MSD of oxygen and bismuth in pure Bi_2O_3 at 1100 K. The MSD of oxygen is increased with the time almost linearly. The MSD of oxygen at final step, 20 $Å^2$, corresponds to the distance to second or third nearest neighbor sites of oxygen. Therefore, oxygen atoms are considered to be moved enough. On the other hand, the bismuth atoms were not moved. These results correspond well to experimental reports in pure δ-Bi_2O_3. Figure 5(b) shows the diffusion coefficients of oxygen estimated from the MSD with respect to the simulation time. After 20 ps, the diffusion coefficients became about 1×10^{-9} m^2s^{-1}. Previous first-principles MD work in pure Bi_2O_3 on the similar condition reported that the order of magnitude can be estimated at using a simulation lasting a few of tens of ps [10]. Therefore, the time of simulation is considered to be enough to estimate the diffusion coefficients.

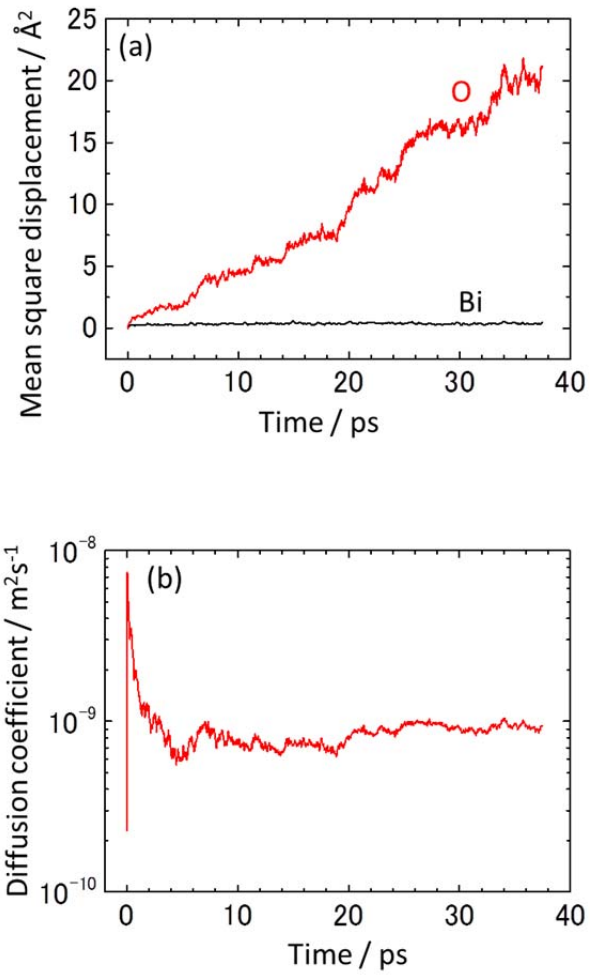

Figure 5. (a) Mean square displacement of bismuth and oxygen in pure Bi_2O_3 at 1100 K

(b) Diffusion coefficients of oxygen in pure Bi_2O_3 at 1100 K

Figure 6 shows MSDs of the first-principles MD simulations on other conditions or other compositions. In the case of low M_2O_3 concentration at high temperature simulation, cations diffused as shown in Figure 6(a) as well. This case is not suited to understand the real oxide ionic conductors. High M_2O_3 concentration or low temperature simulation revealed step-like movement of oxygen as shown in Figure 6(b). This case has much error to estimate diffusion coefficients. In the case of less MSD than 3 $Å^2$, we considered that oxygen atoms are not moved enough and diffusion coefficients have much error. MSD of 3 $Å^2$ means that half of 48 oxygen atoms in the supercell are moved to nearest neighbor sites. These two types of simulations, diffused cation and hardly moved oxygen, were removed in the following analysis.

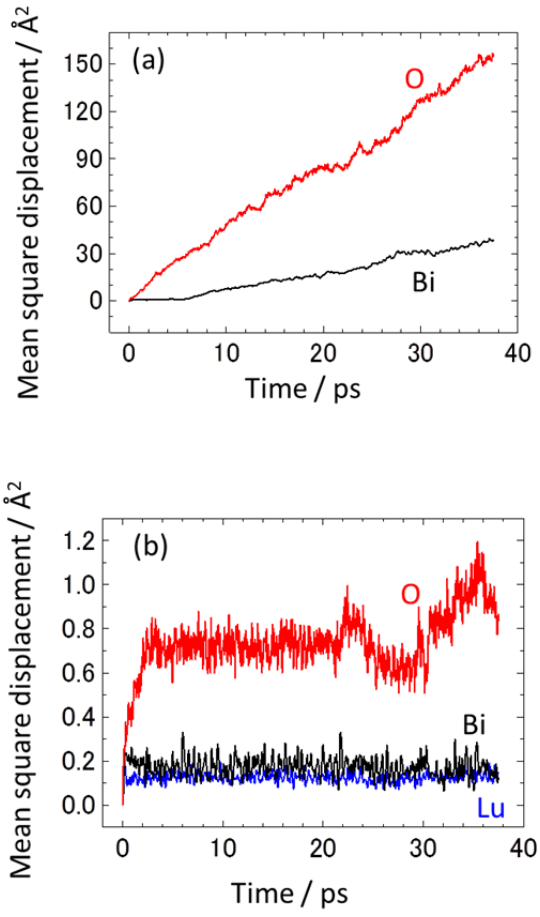

Figure 6. MSDs of the first-principles MD simulations. (a) MSD of pure Bi_2O_3 at 2100 K (b) 50 mol%-Lu_2O_3 Bi_2O_3 at 1100 K

To compare with experiments, the diffusion coefficients were converted to the ionic conductivity. According to the Nernst-Einstein relation of a charged particle, the ionic conductivity at temperature T, σ_ξ can be given by

$$\sigma_\xi = \frac{D_\xi q^2 c}{k_B T}, \tag{20}$$

where k_B denotes the Boltzmann constant. q and c are the ionic charge and ionic concentration of oxygen. The estimated oxide ionic conductivity of pure δ-Bi_2O_3, σ_O is 2.05×10^2 $\Omega^{-1}m^{-1}$ at 1100 K with $q = 2e = 3.204 \times 10^{-19}$ C, where e is the elementary charge. This value agrees well with experimental ionic conductivity of pure δ-Bi_2O_3, 2×10^2 $\Omega^{-1}m^{-1}$ at 1100 K [42] as shown in Figure 7. Figure 8 shows the comparison with experimental ionic conductivity in Bi_2O_3-Y_2O_3 system. Opened squares mean estimated values from first-principles MD and solid lines mean experimental values [14]. The ionic conductivities obtained from first-principles MD represent good agreement with extrapolation of reported experimental values. Good agreements were found also in other reported solutes, Er, Gd and Dy [15–17]. These good agreements with experiments suggest that the simulation time is enough to estimate ionic conductivities.

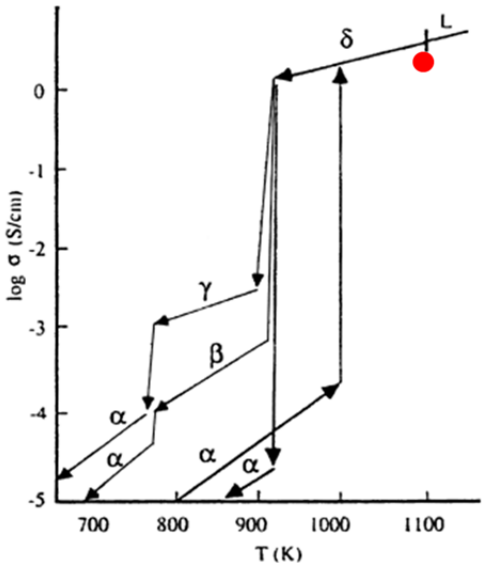

Figure 7. Comparison of calculated and experimental [42] data of pure Bi_2O_3. Red circle is calculated ionic conductivity.

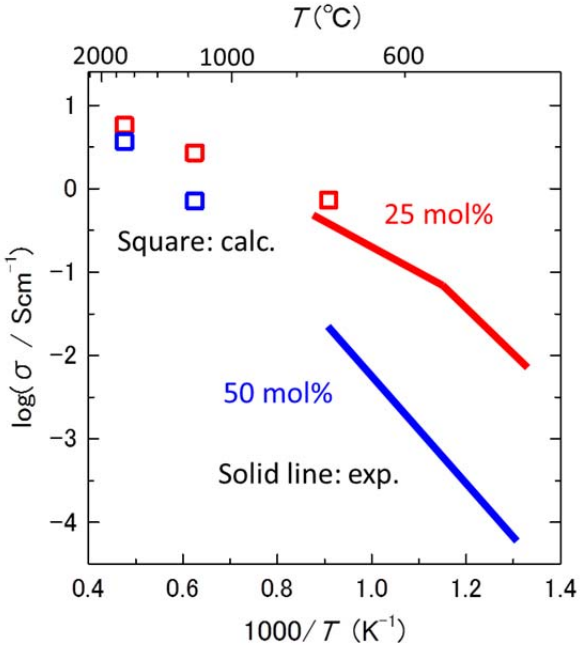

Figure 8. Comparison of calculated and experimental [14] data in Bi_2O_3-Y_2O_3 system

In order to investigate the feature of ionic conductivity in Bi_2O_3–M_2O_3 system with experiments, the activation energy E_a and pre-exponential term D_0 in Arrhenius equation were calculated. The Arrhenius equation of diffusion coefficients was given by

$$D = D_0 \exp(-\frac{E_a}{k_B T}), \quad (21)$$

where k_B and T denotes Boltzman constant and temperature, respectively. In this study, E_a and D_0 were estimated by linear fitting of D at several temperatures.

The calculated activation energy of pure Bi_2O_3 is 44 kJ / mol, which represents good agreement with reported experimental value, 38.5 kJ / mol [42]. Figure 9 shows the calculated E_a and D_0 against solute concentration. The difference between solutes could not been found clearly. On the other hand, the concentration dependence was found; E_a is increasing with the increase of concentration and D_0 is almost constant from 0 to 50 mol%. This tendency is observed also in experimental reports as shown in Figure 10 [43]. The conditions of the MD simulations in this work are enough to capture the rough tendency, concentration dependence.

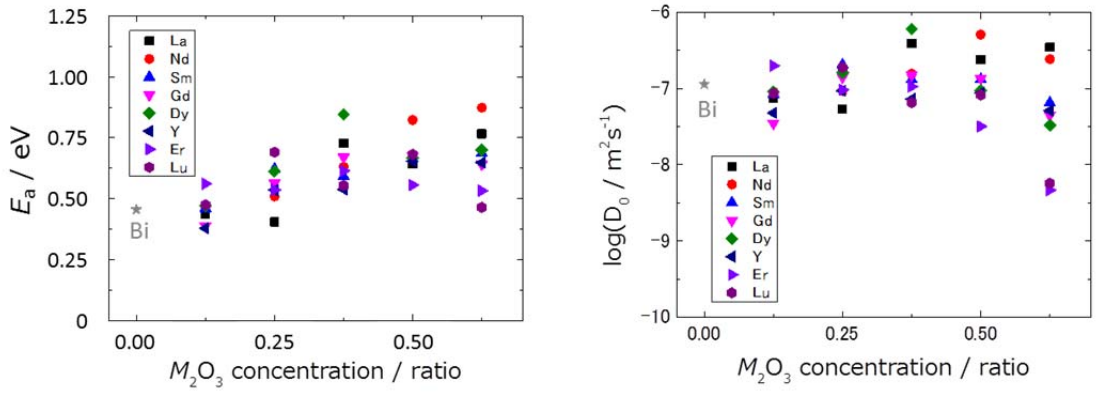

Figure 9. Activation energy E_a and pre-exponential term D_0 in the Arrhenius equation against solute concentration

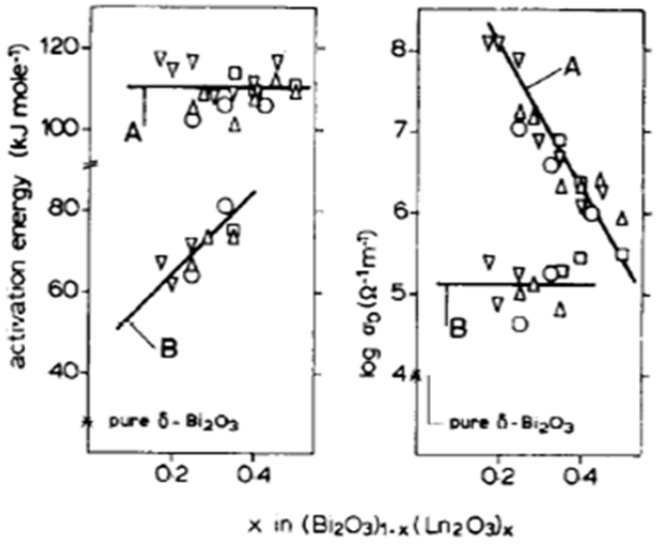

Figure 10. Experimental activation energy E_a and pre-exponential term D_0 [43]. A and B are for low and high temperature range, respectively. B corresponds to the temperature of MD simulations in this work.

Figure 11 shows ionic conductivities in Bi_2O_3-Y_2O_3 and Bi_2O_3-Er_2O_3 systems estimated from first-principles MDs. The plots of high solutes concentration do not represent linear shape because the simulations with low ionic conductivity have much error. The tendency that diffusion coefficients become low with the increase of solute concentration was found in all solutes. This tendency agrees with previous reports of solutes Y, Er, Gd and Dy [14–17]. Figure 12 shows concentration dependence of diffusion coefficients. The diffusion coefficients decrease with the increase of solutes concentration as describe before. The order of solutes is in descending order of their ionic radius. Besides concentration dependence, it is observed that the diffusion coefficients tend to be large when the ionic radius of solutes is large. To understand ionic conductivity in the Bi_2O_3-M_2O_3 systems, other factors must be investigated.

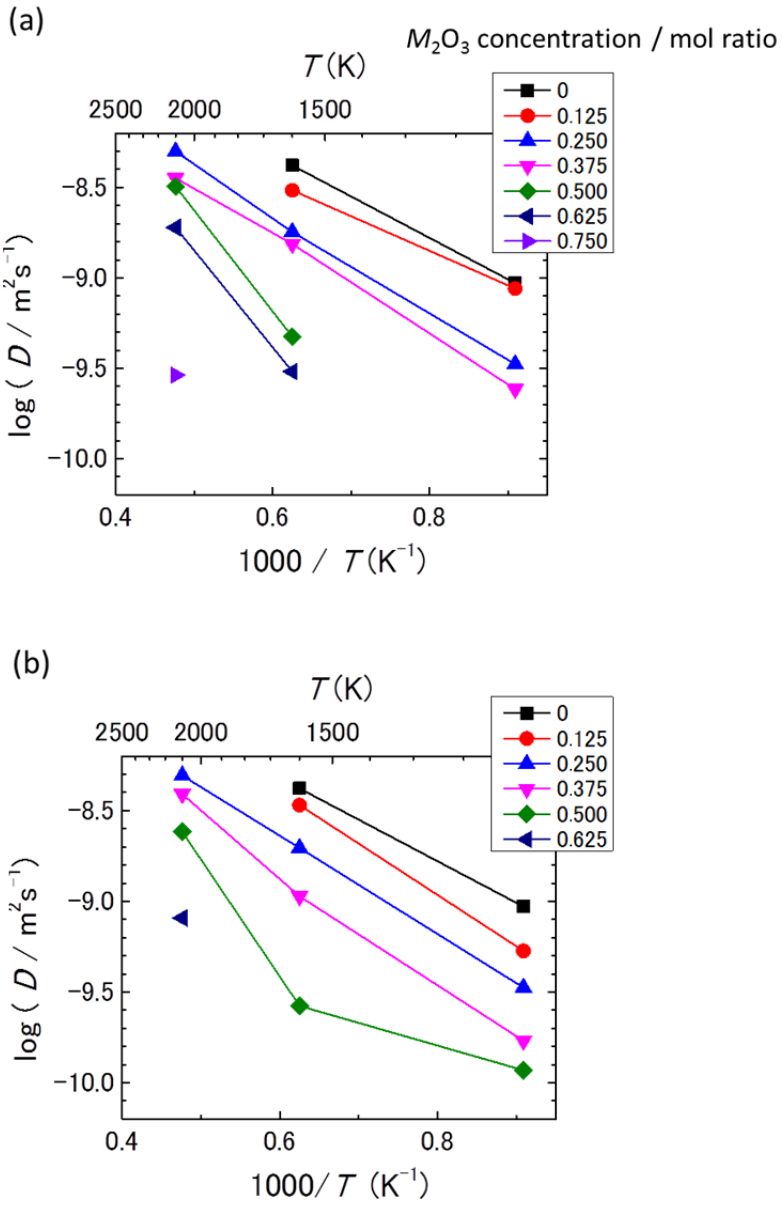

Figure 11. Arrhenius plots of diffusion coefficients in Bi_2O_3-M_2O_3 systems. *M* is (a) Y and (b) Er

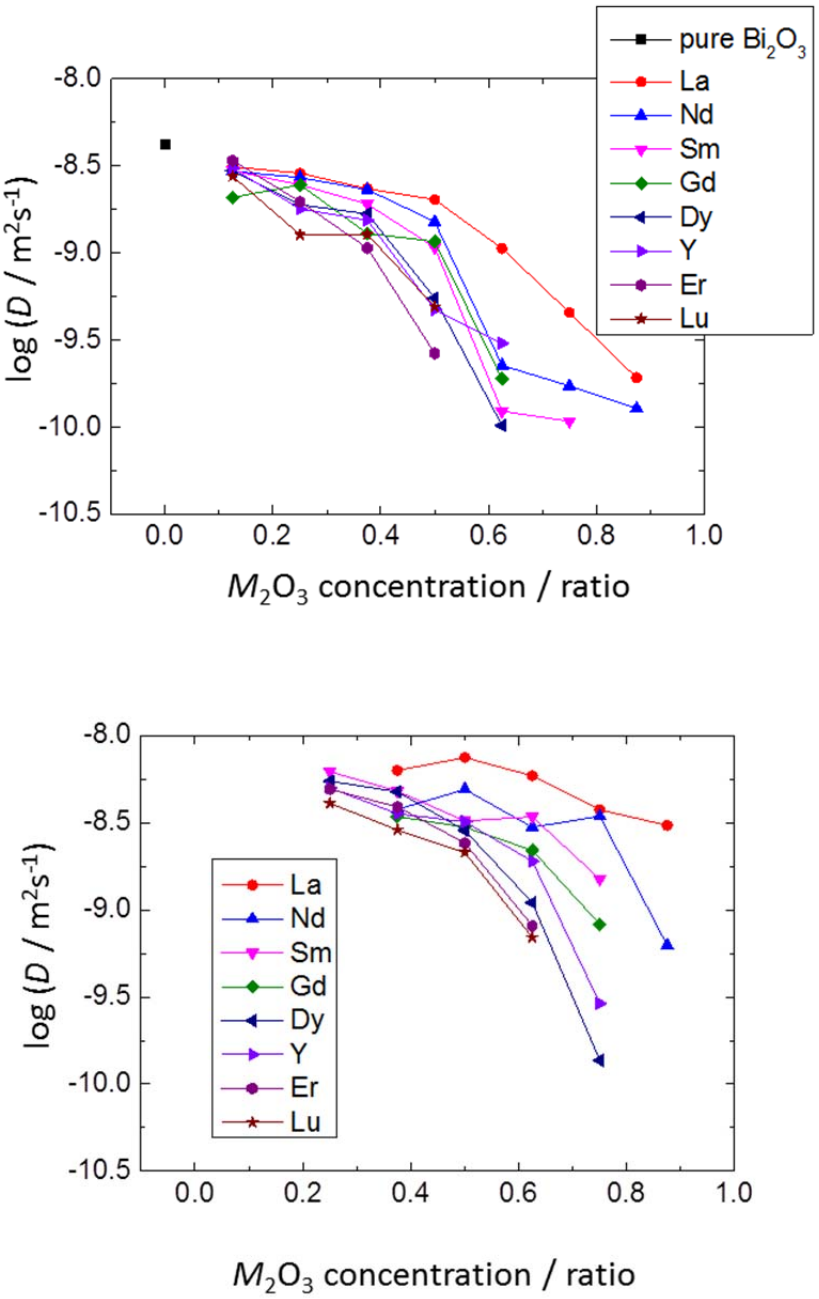

Figure 12. Concentration dependence of diffusion coefficients

3-1-2. Oxygen distribution

In order to understand ionic conductivity in the Bi_2O_3-M_2O_3 systems, the oxygen distribution density was investigated. The oxygen distribution density was evaluated on a 32×32×32 mesh in the 80-atom simulation cell to visualize the oxygen distribution. Figure 13 shows cross-sectional views of the oxygen distribution density in pure Bi_2O_3 at 1600 K from [100] direction. Although all of distribution densities of 8c sites were not same because the simulation time is not enough from the view point of convergence of oxygen distribution densities, however, the typical features can be captured. As can be seen in Figure 13, the distribution of oxygen is centered at 8c sites and expansion to 32f sites of the distribution density is found. This corresponds to previous reports [7].

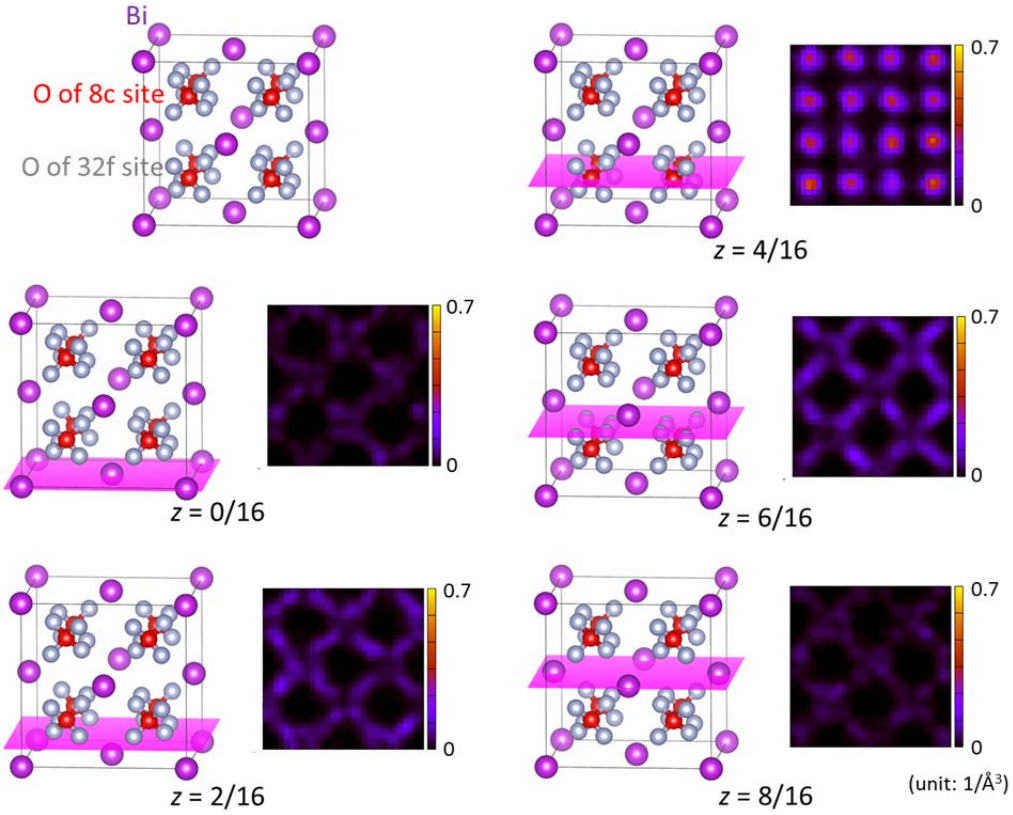

Figure 13. Cross-sectional views of the oxygen distribution density in pure Bi_2O_3 at 1600 K from [100] direction

Figure 14 shows cross-sectional views in the typical 8c sites of the oxygen distribution density in Y_2O_3 25 mol% at 1600 K from [100] direction. The more biased distribution was observed in 8c sites than that of pure Bi_2O_3. Compared to the left image of cation sulattiace, high oxygen distribution densities were shown in the sites near yttrium ions. This biased distribution was found in all of other solutes. In order to understand these biased oxygen distributions, two types of distribution functions, radial and angular distribution functions, were calculated.

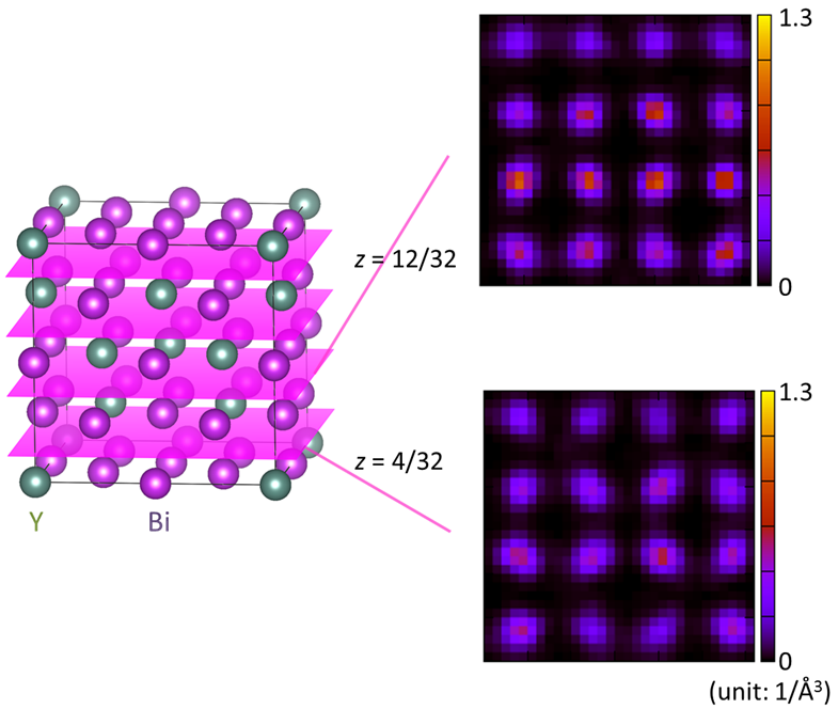

Figure 14. Cross-sectional views in the typical 8c sites of the oxygen distribution density in Y_2O_3-25 mol% Bi_2O_3 at 1600 K from [100] direction

The radial distribution function $g(r)$ is given by

$$g(r) = \frac{1}{N}\sum_i \frac{1}{\rho}\frac{\mathrm{d}n_i(r)}{4\pi r^2 \mathrm{d}r}, \quad (22)$$

where N and ρ denotes the number of particles and the density of particle in the system, respectively. $\mathrm{d}n_i(r)$ is the number of particles in the spherical shell whose radii are r and $r + \mathrm{d}r$ from some particle *i*. In MD simulation, $g(r)$ is taken as average during the all simulation steps. $g(r)$ is total radial distribution function when all of particles are considered. The partial radial distribution function of atom A and B, $g_{AB}(r)$ is given by

$$g_{\mathrm{AB}}(r) = \frac{1}{N_{\mathrm{A}}}\sum_i \frac{1}{\rho_{\mathrm{B}}}\frac{\mathrm{d}n_i^{\mathrm{B}}(r)}{4\pi r^2 \mathrm{d}r}, \quad (23)$$

where N_{A} and ρ_{B} is the number of atom A and the density of atom B in the system, respectively. $\mathrm{d}n_i^{\mathrm{B}}(r)$ is the number of atom B in the spherical shell whose radii is r and $r + \mathrm{d}r$ from some atom *i* of A. This partial radial distribution function is one of the two-body distribution function and therefore, commutative between A and B, i.e. $g_{\mathrm{AB}}(r) = g_{\mathrm{BA}}(r)$. In this study, the partial radial distribution function was calculated the $\mathrm{d}r$ being set to 0.01 Å. In the partial radial distribution function, peak position corresponds to average of the distance between atom species and integral of the function corresponds to coordination number, *CN*, which is defined as the number of atom in some distance from the central atom in this study. The coordination number of A within the distance r, which is the number of B around A, $CN_{\mathrm{AB}}(r)$ is given by

$$CN_{\mathrm{AB}}(r) = \rho_{\mathrm{B}} \int_0^r 4\pi r^2 \, g_{\mathrm{AB}}(r)\mathrm{d}r. \quad (24)$$

Figure 15 shows the partial radial distribution functions of Y_2O_3 25 mol% at 1600 K. The shapes of the partial radial distribution functions of cation-cation and cation-oxygen are similar respectively. However, the peak position and intensity are different and it reflects the local state. Figure 16 shows the partial radial distribution functions of cation-oxygen. The first peak is placed on about 2.3 Å, which corresponds to the distance between Bi and 8c site O in pure δ-Bi_2O_3, 2.45 Å. The intensity of Y-O here is stronger than that of Bi-O. Coordination number up to 3.2 Å, which corresponds to the number of first nearest neighbor oxygen, $CN_{\mathrm{BiO}}(3.2)$ is 5.43 and $CN_{\mathrm{YO}}(3.2)$ is 6.48. This means that oxygen exists more around yttrium than bismuth. On the other hand, the intensity of Y-O between 3 and 4 Å is smaller than that of Bi-O. This area

corresponds to geometric saddle point of δ-Bi_2O_3, *r* equal to about 3.4 Å. These results imply that yttrium attracts and traps oxygen ion. This tendency was observed in other concentrations and other solutes.

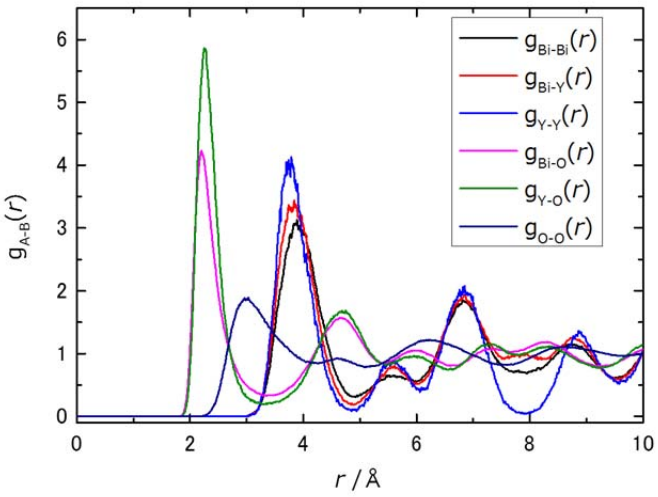

Figure 15. Partial radial distribution functions of Y_2O_3-25 mol% Bi_2O_3 at 1600 K

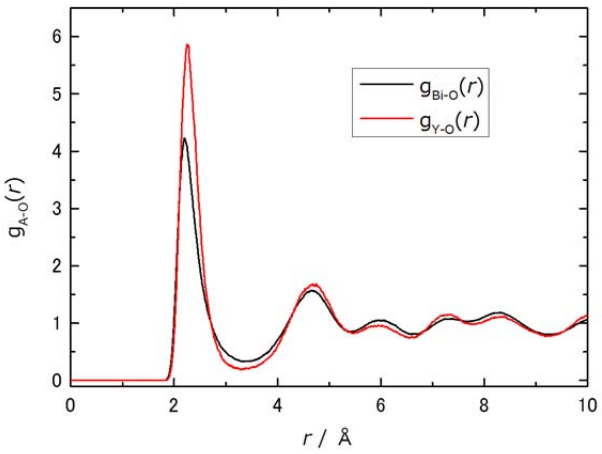

Figure 16. Partial radial distribution functions of *M*-O in Y_2O_3-25 mol% Bi_2O_3 at 1600 K

The partial angular distribution function is given by

$$g_{\mathrm{ABA}}(\theta) = \frac{1}{N}\sum_i \frac{4\pi}{2\pi\sin(\theta)}\frac{\mathrm{d}n_i(\theta)}{\mathrm{d}\theta}, \quad (25)$$

where $\mathrm{d}n_i(\theta)$ denotes the number of the combination of two A atoms and one B atom i which makes the A-B-A angle between θ and $\theta + \mathrm{d}\theta$. N is the total number of the all considered combinations of two A atoms and one B atom. The angular distribution function needs radius range, which was decided by the region of interest. In this work, $g_{\mathrm{OMO}}(\theta)$ was calculated to understand local state in δ-Bi_2O_3-M_2O_3 systems and thus, the radius range was set to 0 to 3.2 Å, which was decided to include only nearest neighbor oxygen from cation.

Figure 17 shows the partial angular distribution functions of Y_2O_3 25 mol% and 75 mol% at 1600 K. The configurations of initial structures of these two compositions are same. The difference is only exchange of Bi and Y. The diffusion coefficients of 25 mol% and 75 mol% are 1.8×10^{-9} m^2s^{-1} and 8.3×10^{-11} m^2s^{-1}, respectively. This difference of diffusion coefficients is appeared also in these two figures. The shape of $g_{\mathrm{OBiO}}(\theta)$ of Y_2O_3 25 mol% is smoother than the other three functions. This is consistent with the result in the partial radial distribution function; oxygen diffuses around Bi mainly.

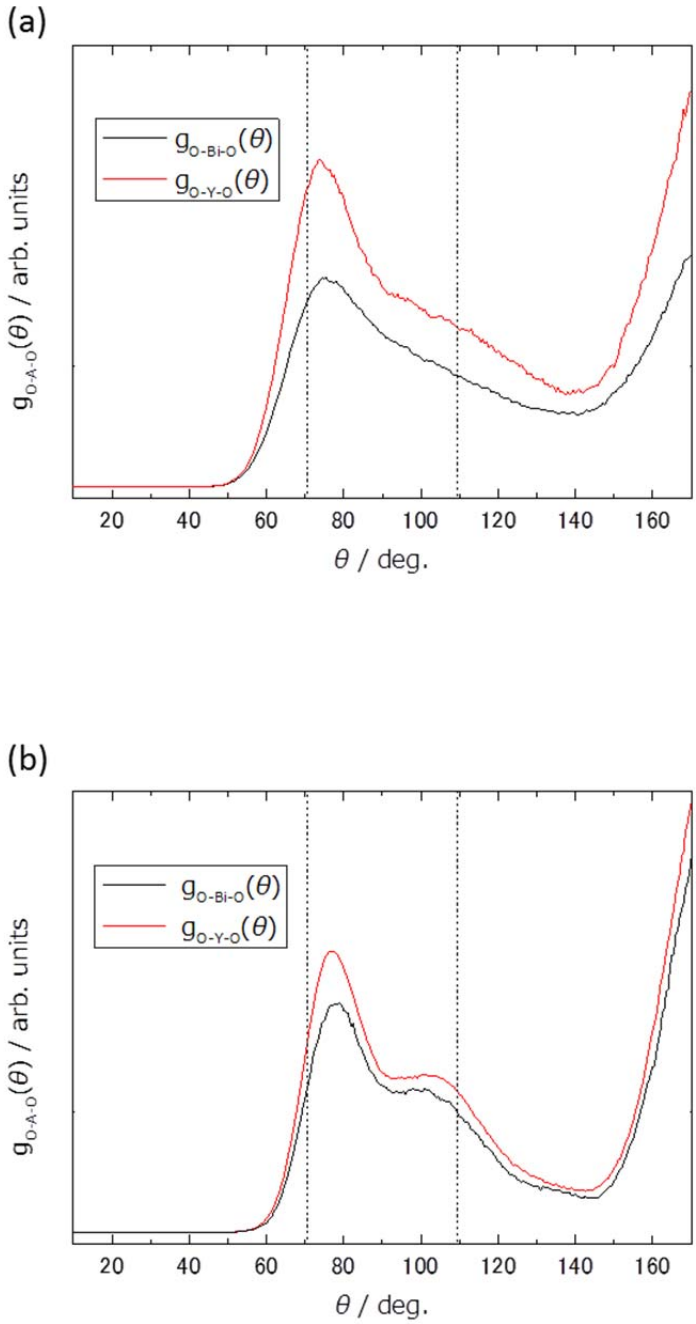

Figure 17. Partial angular distribution functions of O-*M*-O in (a) Y_2O_3-25 mol% Bi_2O_3 and (b) Y_2O_3-75 mol% Bi_2O_3. Broken lines mean the peak position of reportedδ-Bi_2O_3 structure.

The peaks of $g_{OMO}(\theta)$ of reported δ-Bi_2O_3, perfectly oxygen disordered structure, should be placed on 70.5 and 109.5 degree and their intensities are same as shown in the Figure 18(a). However, the partial angular distribution functions of our simulations have a strong peak on about 75 degrees and a weak shoulder peak around 110 degrees. It is found that the function shape differs from that of the perfectly disordered defective fluorite structure in all of Bi_2O_3–M_2O_3 systems in this work. This implies that the local state in Bi_2O_3–M_2O_3 systems is quite different from the perfectly disordered defective fluorite structure during oxygen diffusion. Figure 18(b)-(d) shows $g_{OBiO}(\theta)$ of oxygen ordered defective fluorite structures as well. These figures show that the ratio of the intensities of the two peaks could be changed and imply that local states in Bi_2O_3 –M_2O_3 systems during MD simulation in this work may be something like some oxygen ordered structure.

Figure 19 shows the partial angular distribution functions of the similar structures with a defective fluorite structures, β-Bi_2O_3 and C-type rare-earth structures, with the partial angular distribution function of Y_2O_3 25 mol%. The partial angular distribution function of C-type rare-earth structure was calculated from reported Y_2O_3 structure [44]. The shapes of $g_{OBiO}(\theta)$ and $g_{OYO}(\theta)$ of 25 mol% Y_2O_3 are similar, and therefore, the local states around Bi and Y are also similar. These shapes are similar with $g_{OMO}(\theta)$ of C-type rare-earth structure. The C-type rare earth structure is bcc structure but it can be considered as distorted defective fluorite structure where oxygen is ordered. The strong peak and shoulder peak in the MD simulation are good agreement with $g_{OMO}(\theta)$ of C-type rare earth structure. This implies that oxygen in Y_2O_3 25 mol% systems prefers some ordered local state like C-type rare-earth structure as well.

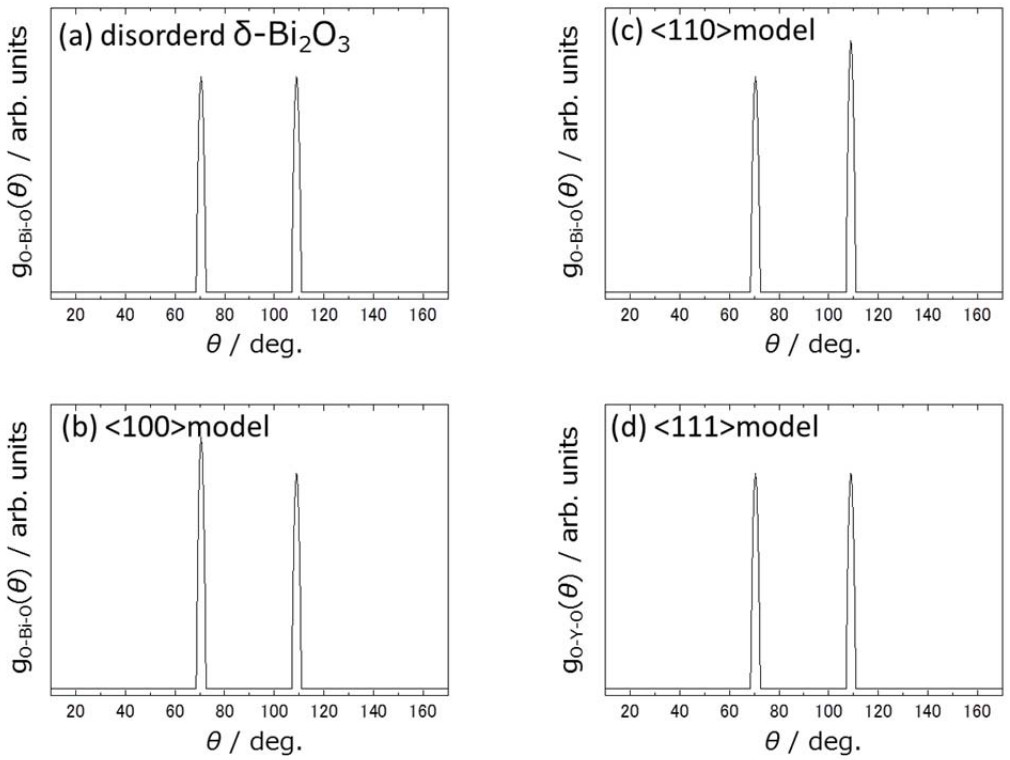

Figure 18. Partial angular distribution functions of (a) perfectly disordered δ-Bi_2O_3, and (b) δ-Bi_2O_3 where oxygen vacancy is placed along <100> direction, (c) <110> direction, and (d) <111> direction

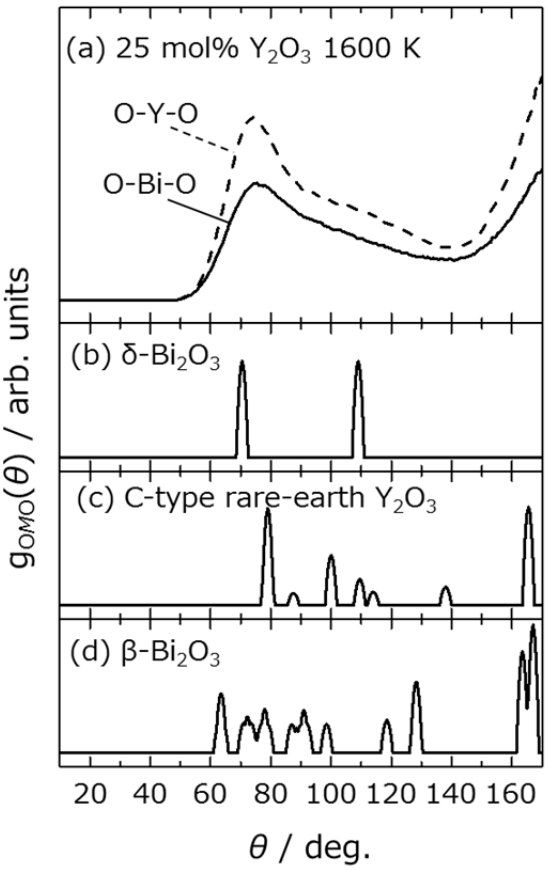

Figure 19. Partial angular distribution functions of (a) 25mol%-Y_2O_3 Bi_2O_3 at 1600 K with (b) the experimental structure of perfectly disorderedδ-Bi_2O_3, (c) C-type rare-earth Y_2O_3, and (d) β-Bi_2O_3

Figure 20 shows the partial angular distribution functions of all solutes 25 mol% at 1600 K. The partial angular distribution functions of the solutes other than La and Nd are similar with the results of Y. Although the partial angular distribution functions of La and Nd seem to be similar with others, they have different features of the partial angular distribution functions, especially the strongest peak position and they cannot be explained by reported oxides of them. They revealed higher diffusion coefficients than other elements which have similar partial angular distribution functions with C-type rare-earth structure. These two oxides have A-type rare-earth structure at ordinary temperatures and pressures [45]. On the other hand, the oxides of solutes other than them have C-type rare-earth structure. These results imply it is effective for improvement of diffusion coefficients that we select the elements prefer to have different local structure from C-type rare-earth structure as solutes.

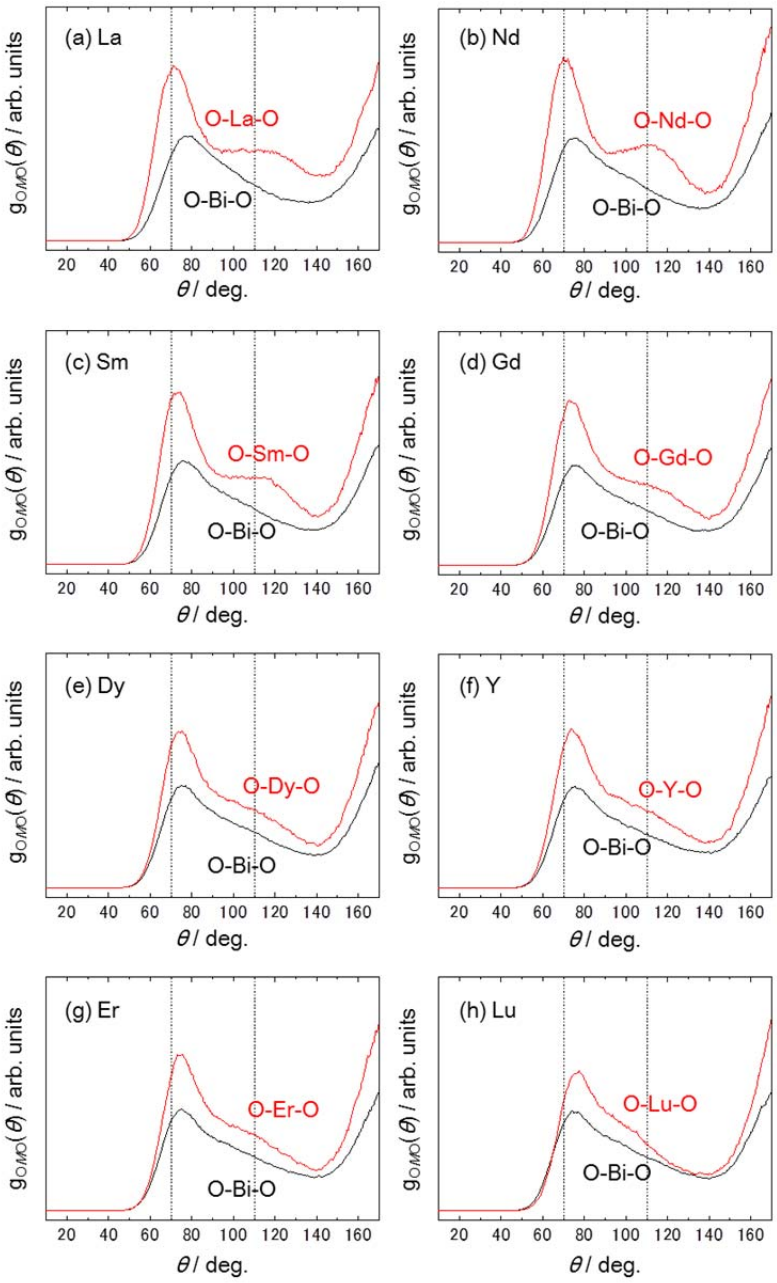

Figure 20. Partial angular distribution functions of the concentration of 25 mol% at 1600 K. Broken lines mean the peak position of reportedδ-Bi_2O_3 structure.

Figure 21 shows the partial angular distribution functions of several temperatures and Y_2O_3 concentrations with the calculated diffusion coefficients. Both of $g_{\mathrm{OBiO}}(\theta)$ and $g_{\mathrm{OYO}}(\theta)$, is smoother with increase of the temperature and decrease of Y_2O_3 concentration. The smoothness of the partial angular distribution function $g_{\mathrm{OBiO}}(\theta)$ corresponds to diffusion coefficients continuously. The value of diffusion coefficients is more than 1×10^{-9} m^2s^{-1} when the $g_{\mathrm{OBiO}}(\theta)$ have no shoulder peak near 110 degree of theta, as shown in Y_2O_3 25 mol% at 1600 K, Y_2O_3 25 mol% at 2100 K, and Y_2O_3 50 mol% at 2100 K. All of the partial angular distribution functions $g_{\mathrm{OBiO}}(\theta)$ are smoother than $g_{\mathrm{OYO}}(\theta)$ at same temperature and composition.

Figure 22 shows the partial angular distribution functions of C-type rare-earth structure Y_2O_3 during MD simulations at several temperatures. These shapes of the partial angular distribution functions look like broadened one of the C-type rare earth structure from experimental report in Figure 20. We can find a broad peak around 140 degree in C-type rare-earth structure and it is observed also in the partial angular distribution function $g_{\mathrm{OBiO}}(\theta)$ of Y_2O_3 75 mol% at 1100 K in Figure 21, implying that Bi has local structures of oxygen like the C-type rare earth structure as well.

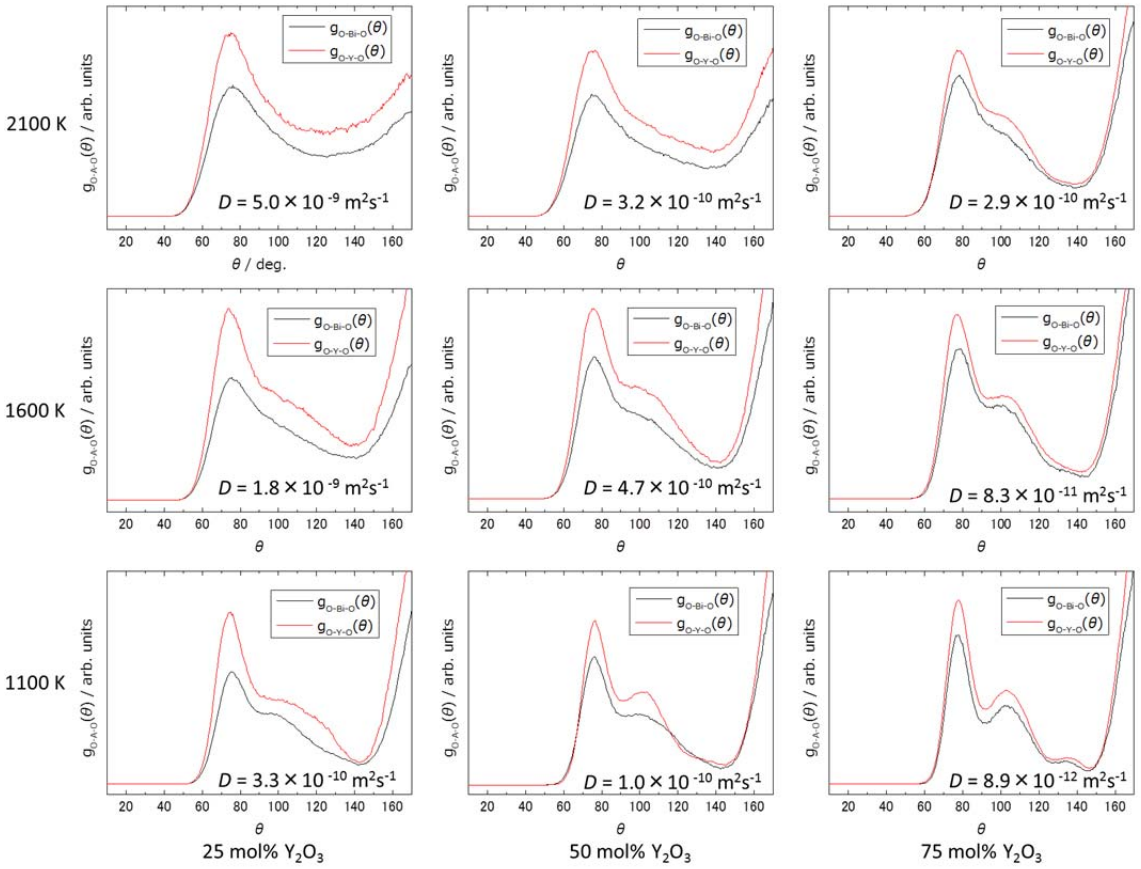

Figure 21. Partial angular distribution functions in Bi_2O_3-Y_2O_3 system at several temperatures with diffusion coefficients

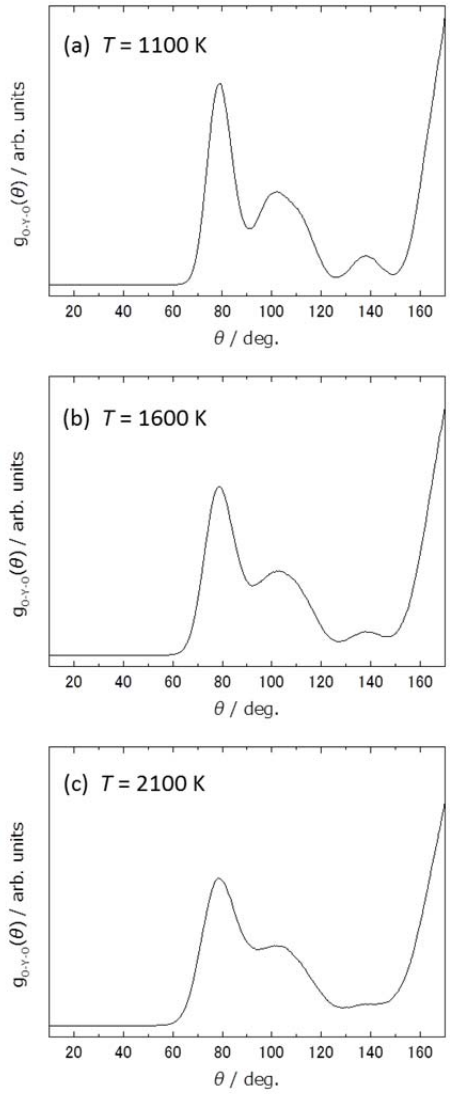

Figure 22. Partial angular distribution functions of C-type rare-earth structure Y_2O_3 during MD simulations

3-1-3. Calculations of cation ordered structures

In the previous section, the oxygen diffuses around Bi ion mainly. Therefore, one of the methods to improve ionic conductivity is to make the diffusion path in which oxygen is not trapped. The results of some typical ordered structures will be shown in this section.

Six structures, three structures of 25 mol% and three structures of 50 mol%, were made as shown in Figure 23. In the left one of 25 mol%, the solute atom yttrium is placed on base-centered position of cation sites in the fluorite unit cell, called as "Y0250_01". Yttrium is placed on basal plane of 2×2×2 supercell in the middle one of 25 mol%, called as "Y0250_02". The right one of 25 mol% is the structure where yttrium is collected along <100> direction, called as "Y0250_03". The diffusion coefficients of Y0250_02 and Y0250_03 are expected to be higher than Y0250_01. In the left one of 50 mol%, Bi and Y are placed one after the other on <100> direction, called as "Y0500_01". The middle one is in the case of <111> direction, called as "Y0500_02" and the right one is <100> direction by two layers, called as "Y0500_03".

The diffusion coefficients of these structures are shown in Table 1. SQS0250 and SQS0500 mean the disordered structure of 25 mol% and 50 mol%, respectively, in which the initial structure was decided by special quasirandom structures. The obtained diffusion coefficients of Y_2O_3 25 mol% are as expected. The Y0500_03 has also larger value of diffusion coefficient than other two structures. On the other hand, there is quite difference between Y0500_01 and Y0500_02. In these two structures, the direction of piled up cations is different. It was reported that oxide ion diffuses along <100> direction in δ-Bi_2O_3 [7] and thus, there may be more paths around Bi in Y0500_02 than Y0500_01.

The orthogonal components of MSD at 37.5 ps are shown in Table 1. It can be found that the simulation time is not enough to reach the convergence of these components from structures symmetry, e.g. the values of x and z direction of Y0250_02 had different values, which should be same. We can find not a small value in the *a* direction of Y0500_03 or the *b* direction of Y0250_02, contrary to expectation. Although it may be because of not reaching convergence, however, it is possible that the trapping effect of solute is not as strong as expected.

Figure 24 shows the partial angular distribution functions of the cation ordered structures. The shapes of the partial angular distribution functions, $g_{\mathrm{OBiO}}(\theta)$ correspond to the diffusion coefficients as same as the case of disordered structures. On the same composition, the local structures and the oxygen diffusion depend on the configuration of cations.

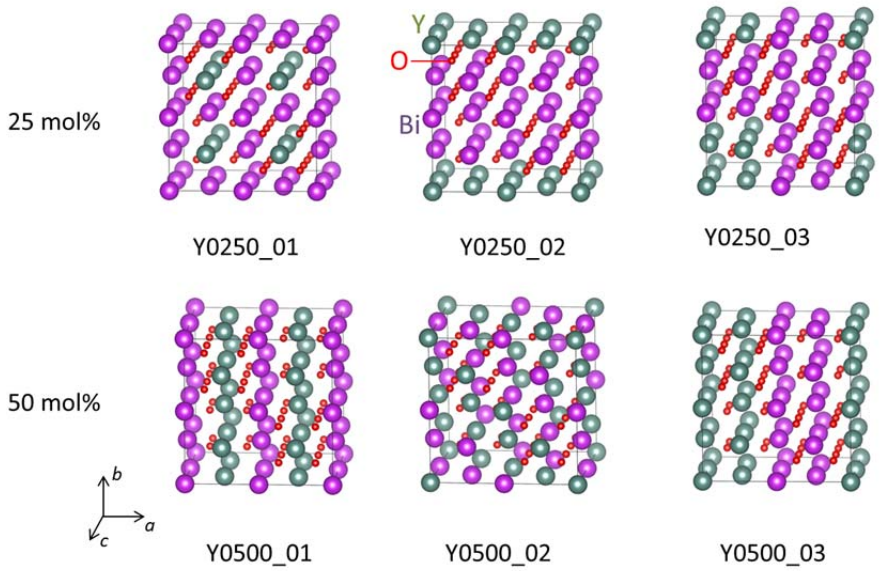

Figure 23. Calculated ordered structures

Table 1. Diffusion coefficients and orthogonal components of MSD in ordered structures and SQSs

	D / m^2s^{-1}	MSD_a / Å^2	MSD_b / Å^2	MSD_c / Å^2
SQS0250	1.79E-09	12.42	12.50	15.45
Y0250_01	1.50E-09	11.29	12.06	10.37
Y0250_02	2.14E-09	14.35	9.78	24.04
Y0250_03	2.35E-09	12.17	24.81	15.92
SQS0500	4.73E-10	3.84	3.44	3.35
Y0500_01	1.09E-10	0.60	0.83	1.03
Y0500_02	6.96E-10	4.44	5.303875	5.91
Y0500_03	1.21E-09	8.32	11.55	7.46

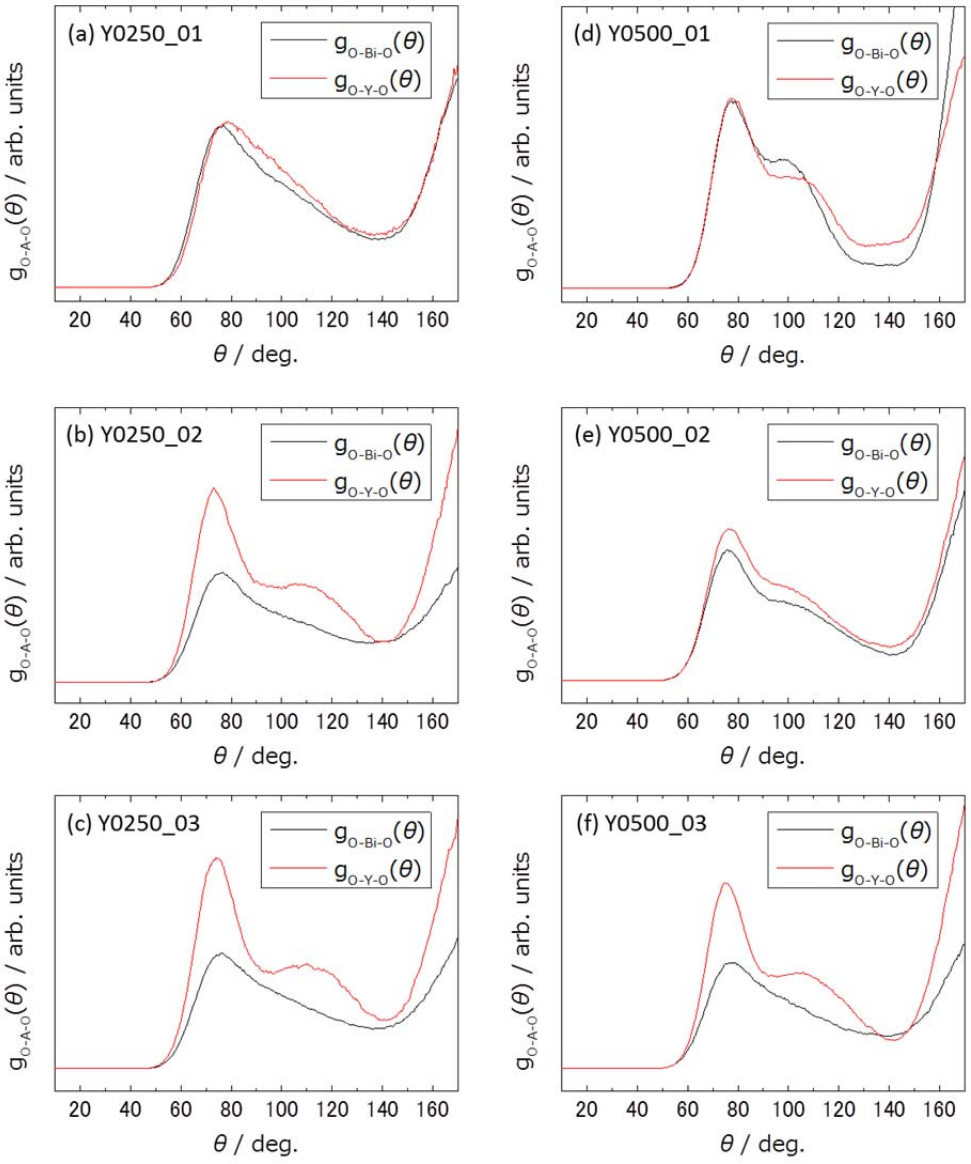

Figure 24. Partial angular distribution functions of ordered structures

The cation configurations like these structures with the solute arranged in a plane are found as the most stable structure in wide composition in chapter 2. Figure 25 shows the most stable structure of Y_2O_3 25 mol% in the chapter 2 and the configuration of cations to be shown as defective fluorite structure. Its cation configuration is same as ordered model of Y0250_02. Although the structures in chapter 2 are ordered about both of oxygen and cation sublattices and it is difficult to calculate the structure where one sublattice is ordered and the other is disordered, however, this implies that the cation ordered cubic structure can be synthesized by some method like low temperature synthesis or thin film.

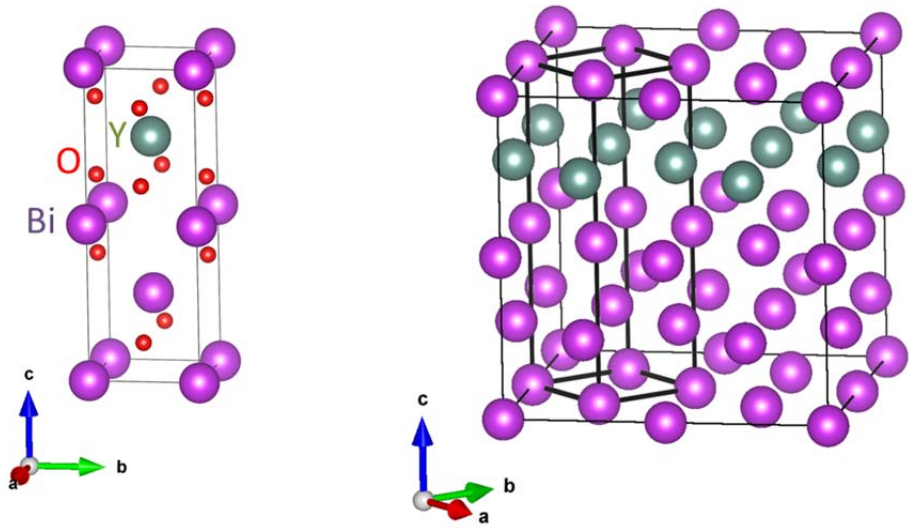

Figure 25. Most stable structure of Y_2O_3-25mol% Bi_2O_3 in chapter 2. Right one is its cation configuration to be shown as defective fluorite structure.

3-2. Analysis and prediction

3-2-1. Analysis of data

In order to investigate the results of MD simulations, informatics analysis was applied. Before analysis, the database was constructed. The system considered in this work is the Bi_2O_3-M_2O_3 pseudobinary system and therefore, the parameters about *M* elements were used as variables, concentration of *M*, atomic mass, electron affinity of *M*, first and second and third ionization energy of *M*, and van der Waals' radius of *M*. As a result of MD simulation, the temperature of MD simulation, the average distance of each element, the coordination number of cations, and the logarithm of diffusion coefficients are used. Moreover, the order-disorder transition temperature from chapter 2 and cell volume are used. Those parameters were summarized in Table 2. The database was constructed only the results of MD simulations of disordered models.

The average distance of each element was calculated from the partial radial distribution functions. All of the partial radial distribution functions were smoothed by Savitzky-Golay filter and peaks were searched where first derivation is equal to zero. This first peak position was used as average distance and all of the atom combinations, Bi-Bi, Bi-*M*, *M*-*M*, Bi-O, *M*-O, and O-O were considered. The coordination numbers were calculated by equation (24). In this section, $CN_{\mathrm{BiO}}(r)$ and $CN_{M\mathrm{O}}(r)$ were calculated and cutoff radius was set to 2.5 and 3.2 Å, which correspond to the values of a near first peak positon and area of the first peak.

Table 2. Variables in analyses

Condition of MD	The temperature during MD	T
Property of M element	Concentration of M	*Conc.*
	Atomic mass of M	*Mass*
	Electron affinity of M	*EA*
	First, second, and third ionization energy of M	*IE1, IE2, IE3*
	van der Waals' radius of M	r
The property from systematic first-principles calculations	The order-disorder transition temperature (from chapter 2)	T_c
	Cell volume	V
The parameters from radial distribution function	Average distance between each element	$Dis._{\text{Bi-Bi}}$, $Dis._{\text{Bi-}M}$, $Dis._{M\text{-}M}$, $Dis._{\text{Bi-O}}$, $Dis._{M\text{-O}}$, $Dis._{\text{O-O}}$
	Coordination number of O around cation (Bi, M) (cutoff radius: 2.5 and 3.2 Å)	$CN_{\text{BiO}}(2.5)$, $CN_{MO}(2.5)$, $CN_{\text{BiO}}(3.2)$, $CN_{MO}(3.2)$
The objective property	Logarithm of diffusion coefficients	$\log D$

Table 3 shows the correlation coefficients between all variables. In general, the high absolute value of the correlation coefficient about more than 0.4 indicates that the two variables have linear correlation. For instance, the volume has high absolute value with all of average distances between elements. This is very consistent because the distance between elements should be longer when the volume becomes larger. However, these values of the correlation coefficients are different; the correlation coefficient between Bi-Bi average distance and the volume is 0.67 and the correlation coefficient between *M*-*M* average distance and the volume is 0.87. This means that the *M*-*M* average distance has stronger linear correlation with the volume than the Bi-Bi average distance, implying that Bi position is more flexible than *M* positon.

The logarithm of diffusion coefficient has high absolute value of correlation coefficients with temperature, Bi-O average distance, and $CN_{\mathrm{BiO}}(2.5)$. However, we cannot conclude that these three parameters have the causal relationship with the diffusion coefficients since the correlation coefficients mean only the linear correlation. Moreover, the high absolute value of correlation coefficients does not always mean that the parameter has linear correlation with other parameter independently. In Table 3, the correlation coefficient between Bi-O average distance and $CN_{\mathrm{BiO}}(2.5)$ is high, 0.71. This implies the possibility that these two values do not have the relation with diffusion coefficients independently. On the other hand, the high correlation coefficient value of temperature is very consistent because of the Arrhenius equation. Therefore, the correlation coefficients about diffusion coefficients result in strong linear correlation of the logarithm of diffusion coefficients with the temperature and, Bi-O average distance or $CN_{\mathrm{BiO}}(2.5)$ or both of them.

Table 3. Correlation functions between all variables

	T	*Conc.*	*Mass*	*EA*	*IE1*	*IE2*	*IE3*	r	T_c	V	log D
T	1.00	0.27	-0.01	0.00	0.01	0.00	0.00	0.00	0.06	-0.15	0.70
Conc.	0.27	1.00	-0.07	-0.09	-0.18	-0.24	-0.10	0.29	0.58	-0.07	-0.34
Mass	-0.01	-0.07	1.00	0.20	-0.01	0.37	0.48	-0.45	-0.06	-0.10	0.03
EA	0.00	-0.09	0.20	1.00	0.87	0.47	0.54	-0.56	0.04	-0.01	0.11
IE1	0.01	-0.18	-0.01	0.87	1.00	0.53	0.27	-0.59	-0.16	-0.25	0.09
IE2	0.00	-0.24	0.37	0.47	0.53	1.00	0.17	-0.91	-0.31	-0.41	0.08
IE3	0.00	-0.10	0.48	0.54	0.27	0.17	1.00	-0.51	-0.03	-0.25	-0.01
r	0.00	0.29	-0.45	-0.56	-0.59	-0.91	-0.51	1.00	0.36	0.57	-0.04
T_c	0.06	0.58	-0.06	0.04	-0.16	-0.31	-0.03	0.36	1.00	0.42	-0.13
V	-0.15	-0.07	-0.10	-0.01	-0.25	-0.41	-0.25	0.57	0.42	1.00	0.20
$Dis._{\text{Bi-Bi}}$	-0.35	0.06	-0.14	-0.19	-0.32	-0.46	-0.29	0.59	0.23	0.67	-0.13
$Dis._{\text{Bi-}M}$	0.19	0.11	-0.18	-0.16	-0.39	-0.70	-0.27	0.83	0.50	0.84	0.39
$Dis._{M\text{-}M}$	0.00	0.05	-0.24	-0.19	-0.41	-0.74	-0.36	0.91	0.40	0.87	0.22
$Dis._{\text{Bi-O}}$	-0.40	0.06	0.07	0.13	0.21	0.27	0.18	-0.34	-0.01	-0.40	-0.65
$Dis._{M\text{-O}}$	-0.33	0.12	-0.23	-0.13	-0.41	-0.81	-0.27	0.94	0.46	0.83	-0.16
$Dis._{\text{O-O}}$	0.28	0.52	-0.10	-0.03	-0.22	-0.32	-0.23	0.45	0.62	0.57	0.06
$CN_{\text{BiO}}(2.5)$	-0.81	-0.09	0.02	0.04	0.14	0.18	0.13	-0.26	-0.19	-0.36	-0.82
$CN_{MO}(2.5)$	-0.32	-0.25	0.20	0.24	0.44	0.70	0.38	-0.90	-0.38	-0.75	-0.35
$CN_{\text{BiO}}(3.2)$	-0.29	-0.32	0.18	0.25	0.37	0.51	0.30	-0.62	-0.31	-0.53	-0.35
$CN_{MO}(3.2)$	-0.57	-0.84	0.04	0.14	0.11	0.01	0.18	-0.09	-0.37	0.14	-0.02
log D	0.70	-0.34	0.03	0.11	0.09	0.08	-0.01	-0.04	-0.13	0.20	1.00

	$Dis._{\text{Bi-Bi}}$	$Dis._{\text{Bi-}M}$	$Dis._{M\text{-}M}$	$Dis._{\text{Bi-O}}$	$Dis._{M\text{-O}}$	$Dis._{\text{O-O}}$	$CN_{\text{BiO}}(2.5)$	$CN_{MO}(2.5)$	$CN_{\text{BiO}}(3.2)$	$CN_{MO}(3.2)$	log D
T	-0.35	0.19	0.00	-0.40	-0.33	0.28	-0.81	-0.32	-0.29	-0.57	0.70
Conc.	0.06	0.11	0.05	0.06	0.12	0.52	-0.09	-0.25	-0.32	-0.84	-0.34
Mass	-0.14	-0.18	-0.24	0.07	-0.23	-0.10	0.02	0.20	0.18	0.04	0.03
EA	-0.19	-0.16	-0.19	0.13	-0.13	-0.03	0.04	0.24	0.25	0.14	0.11
IE1	-0.32	-0.39	-0.41	0.21	-0.41	-0.22	0.14	0.44	0.37	0.11	0.09
IE2	-0.46	-0.70	-0.74	0.27	-0.81	-0.32	0.18	0.70	0.51	0.01	0.08
IE3	-0.29	-0.27	-0.36	0.18	-0.27	-0.23	0.13	0.38	0.30	0.18	-0.01
r	0.59	0.83	0.91	-0.34	0.94	0.45	-0.26	-0.90	-0.62	-0.09	-0.04
T_c	0.23	0.50	0.40	-0.01	0.46	0.62	-0.19	-0.38	-0.31	-0.37	-0.13
V	0.67	0.84	0.87	-0.40	0.83	0.57	-0.36	-0.75	-0.53	0.14	0.20
$Dis._{\text{Bi-Bi}}$	1.00	0.57	0.64	-0.34	0.70	0.30	-0.06	-0.54	-0.56	0.12	-0.13
$Dis._{\text{Bi-}M}$	0.57	1.00	0.83	-0.58	0.72	0.62	-0.60	-0.87	-0.74	-0.10	0.39
$Dis._{M\text{-}M}$	0.64	0.83	1.00	-0.47	0.87	0.57	-0.41	-0.88	-0.63	0.07	0.22
$Dis._{\text{Bi-O}}$	-0.34	-0.58	-0.47	1.00	-0.22	0.00	0.71	0.53	0.84	0.02	-0.65
$Dis._{M\text{-O}}$	0.70	0.72	0.87	-0.22	1.00	0.48	-0.08	-0.75	-0.49	0.16	-0.16
$Dis._{\text{O-O}}$	0.30	0.62	0.57	0.00	0.48	1.00	-0.41	-0.67	-0.29	-0.57	0.06
$CN_{\text{BiO}}(2.5)$	-0.06	-0.60	-0.41	0.71	-0.08	-0.41	1.00	0.64	0.60	0.38	-0.82
$CN_{MO}(2.5)$	-0.54	-0.87	-0.88	0.53	-0.75	-0.67	0.64	1.00	0.72	0.23	-0.35
$CN_{\text{BiO}}(3.2)$	-0.56	-0.74	-0.63	0.84	-0.49	-0.29	0.60	0.72	1.00	0.26	-0.35
$CN_{MO}(3.2)$	0.12	-0.10	0.07	0.02	0.16	-0.57	0.38	0.23	0.26	1.00	-0.02
log D	-0.13	0.39	0.22	-0.65	-0.16	0.06	-0.82	-0.35	-0.35	-0.02	1.00

As another procedure of unsupervised learning, PCA was performed. The database was normalized to have zero-mean and unit-variance about all parameters before PCA. Table 4 and Figure 26 show the proportion of variance and the cumulative proportion. In this work, the PCs were considered up to PC4 because the cumulative proportion becomes 81 %, over 80 %. In order to visualize the feature of variables relationship, all biplots of the combinations up PC4 were investigated and typical results will be shown. Figure 27(a) shows biplots of PC1 and PC2. It is found that the logarithm of diffusion coefficients is placed along same direction from origin with temperature and concentration, and along opposite direction with average distance of Bi-O, $CN_{\mathrm{BiO}}(2.5)$, and $CN_{MO}(3.2)$. Some of them are consistent with the results of the correlation coefficients. However, the logarithm of diffusion coefficients has little loading of PC1. In this case, other PCs could be useful to capture the characteristic of database. Figure 27(b) shows biplots of PC2 and PC3, which have 31 % of combined proportion of variance and this can be considered to have enough information to capture the database characteristic. In this figure, order-disorder temperature, T_c is placed along almost opposite side of the logarithm of diffusion coefficients. This information cannot be obtained only by figure 27(a) and we should pay attention to the values of proportion of variance and biplots based on these values. Figure 28 shows values of $\mathrm{VIP}_{\mathrm{PCA}}$ where a target variable was set to the logarithm of diffusion coefficients. This result shows similar result with that of correlation coefficient. However, PCA revealed more importance of concentration and T_c than the analysis of the correlation coefficients.

Table 4. Proportion of variance and the cumulative proportion in PCA

The number of PC	Proportion of variance	Cumulative proportion
PC 1	0.428	0.428
PC 2	0.181	0.609
PC 3	0.130	0.739
PC 4	0.070	0.809
PC 5	0.057	0.866
PC 6	0.051	0.917
PC 7	0.023	0.940
PC 8	0.017	0.957
PC 9	0.014	0.971
PC 10	0.010	0.981
PC 11	0.006	0.987
PC 12	0.005	0.991
PC 13	0.003	0.994
PC 14	0.002	0.996
PC 15	0.002	0.998
PC 16	0.001	0.999
PC 17	0.001	0.999
PC 18	0.000	1.000
PC 19	0.000	1.000
PC 20	0.000	1.000
PC 21	0.000	1.000

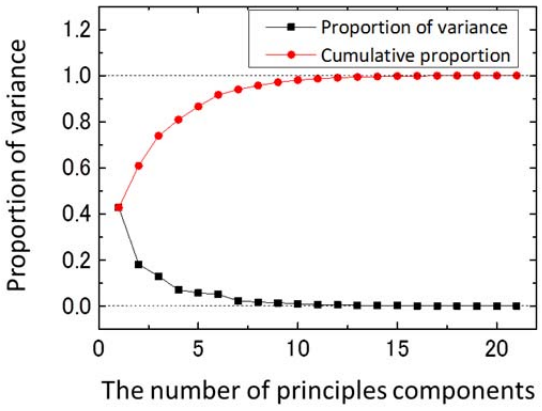

Figure 26. Proportion of variance and the cumulative proportion against the number of principle components

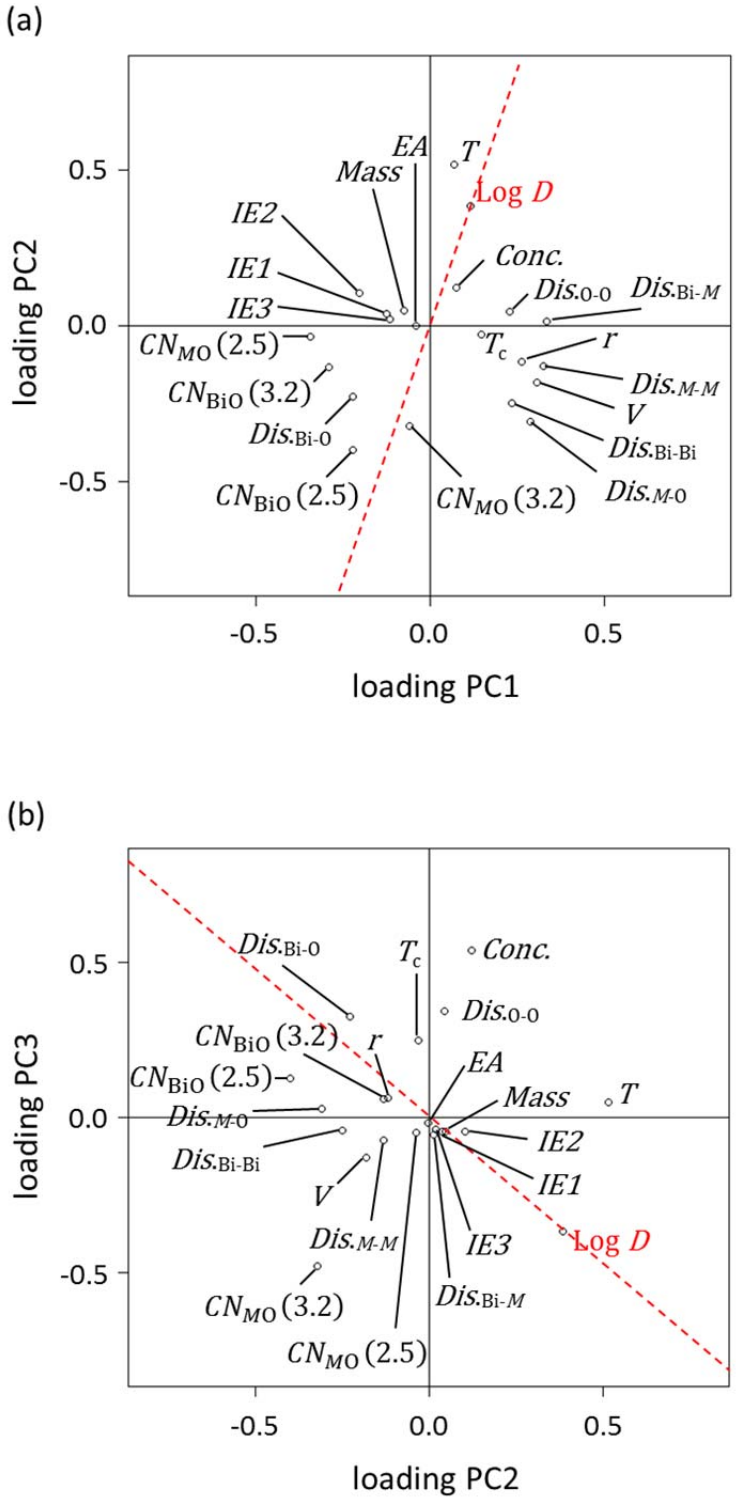

Figure 27. PCA biplots of (a) PC1 and PC2, and (b)PC2 and PC3

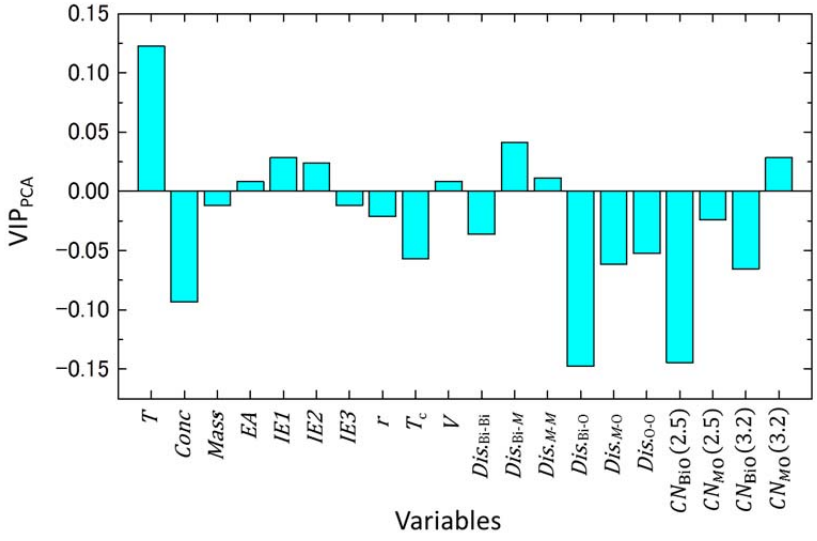

Figure 28. Values of VIP_{PCA} in the database. Target variable was set to diffusion coefficients.

Hereafter, the results of the supervised learnings will be shown in order to reveal the effect of the variables to the diffusion coefficients. The goodness of the regressions was checked by the RMSE of data and 5-fold CV score. Moreover, we attempted to apply the regression equations to the data of the ordered structures in order to check extrapolation power, although all of the regression equations were made from the database of only the disordered structures. If the radial distribution functions, which can distinguish ordered and disordered structures in the considered parameters, can capture the feature about diffusion coefficients in this system including atom configurations, the extrapolation to the ordered structures is expected to be good.

Figure 29 shows OLSR results, where red circles and blue circles are the data of the disordered structures to perform regression and the ordered structures, respectively. A grey line means that the predicted and calculated values are same. The RMSE of dataset was 0.126 and 5-fold CV score was 0.164. The 5-fold CV score is quite higher compared to the RMSE of dataset and this regression is over-fitting. Thus, this regression is considered to be unable to capture the characteristic of the logarithm of diffusion coefficients in the Bi_2O_3-M_2O_3 systems. Moreover, blue circles are far from

the line where the predicted and calculated values are same. RMSE of the data of the ordered structures was also very high, 1.01. This means that the regression equation cannot be applied to ordered structures.

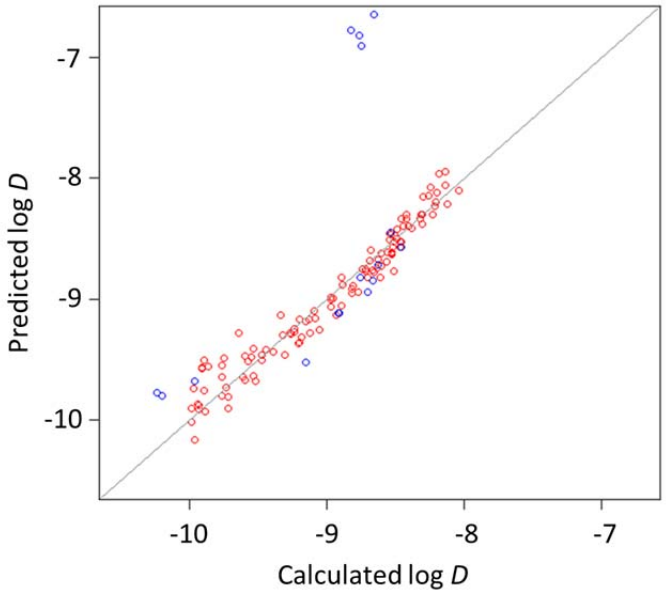

Figure 29. Comparison of predicted and calculated log *D* in OLSR with all variables

Figure 30 shows the regression result of OLSR with variable selection by AIC. The RMSE of dataset was 0.134 and 5-fold CV score was 0.145 and the 5-fold CV score was not higher compared to the result of OLSR with all variables. This result indicates that the over-fitting was inhibited. The predicted values of the ordered structures were also closer to the calculated values than that of OLSR with all variables and RMSE of the data of the ordered structures was 0.316. This result implies that this regression can capture the characteristic of log D in the system including atomic configurations better than OLSR with all variables. The regression equation was given as

$$\log D = 0.05 - 0.91conc. + 0.69T - 0.25CN_{\mathrm{BiO}}(3.2) - 0.33CN_{MO}(3.2) + 0.20\mathrm{distBiM} - 0.15\mathrm{distOO} + 0.07\mathrm{Tc}. \quad (26)$$

The coefficients are the values after database was normalized and they correspond to contribution to the regression of the logarithm of diffusion coefficients. In OLSR with the variables selection by AIC, concentration is the most contributed variable and temperature is second one. Although it feels strange that the coefficient of temperature is positive, however, it is consistent with Arrhenius equation since T has strong linear correlation with negative inverse, -1/T in the considered temperature range in this work.

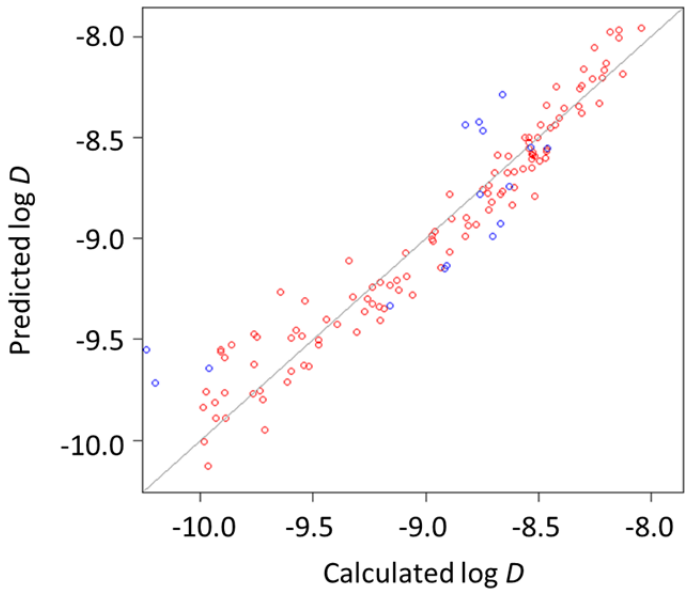

Figure 30. Comparison of predicted and calculated log D in OLSR with variables selection by AIC

Figure 31 shows the regression result of LASSO. The RMSE of dataset and 5-fold CV score were very close values, 0.155 and 0.162, respectively. The predicted values of the ordered structures were close to the calculated values. The RMSE of the data of the ordered structures was 0.213. This implies that the characteristic of the diffusion coefficients is captured very well in this system including atomic configurations. The regression equation was given as

$$\log D = -0.44conc. + 0.46T + 0.015distBiM - 0.18\mathrm{distBiO} - 0.31CN_{\mathrm{BiO}}(2.5). \quad (27)$$

Selected variables differ from those of OLSR with AIC. The variables selected by a number of methods can be considered to be more important than others. Moreover, the variables selected by LASSO are considered to capture the characteristic of diffusion coefficients better because of the values of the RMSEs and 5-fold CV score.

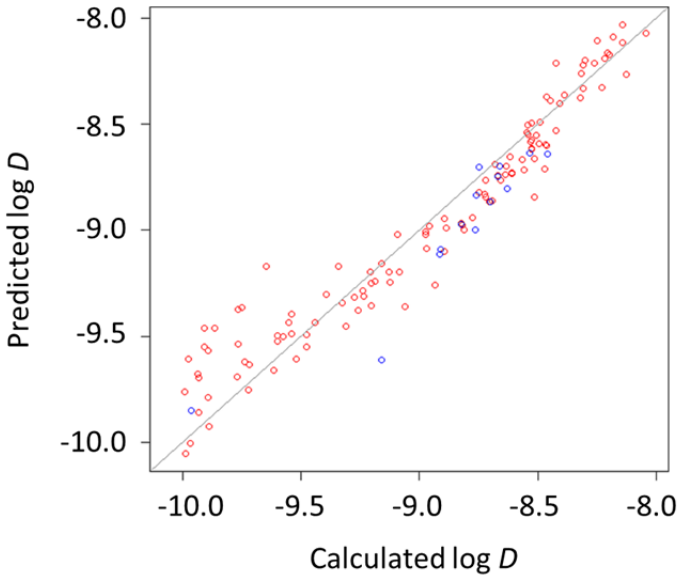

Figure 31. Comparison of predicted and calculated log D in OLSR with variables selection by LASSO

Figure 32 shows the result of PLSR. The RMSE of training dataset was 0.150 and 5-fold CV score was 0.162. Considering these values, this PLSR could be considered to be better than OLSR with LASSO. However, the RMSE of the data of the ordered structures was 0.391, which indicates that the characteristic of the ordered structures could not be captured well by PLSR. The coefficients of original variables in PLSR are shown in Table 5. These values are after normalization of database. Concentration, temperature and $CN_{\mathrm{BiO}}(2.5)$ seem to be more contributed than others. Figure 33 shows the $\mathrm{VIP}_{\mathrm{PLSR}}$. The variables which reveal more than one of $\mathrm{VIP}_{\mathrm{PLSR}}$ are concentration, temperature, average distance of Bi-*M*, average distance of Bi-O, $CN_{\mathrm{BiO}}(2.5)$, and $CN_{\mathrm{BiO}}(3.2)$. The average distance of Bi-O has the third highest value of $\mathrm{VIP}_{\mathrm{PLSR}}$ but does not have high coefficients. This is because average distance of Bi-O can be displaced by $CN_{\mathrm{BiO}}(2.5)$ in the regression equation because of the high correlation coefficient of them shown in Table 3. This is one of the weaknesses of PLSR. The PLSR can make good regression replying the target variable because of its feature, max covariance between target and other variables. However, the coefficients often have no meanings. Thus, we should check $\mathrm{VIP}_{\mathrm{PLSR}}$ and compare the result with that of other methods.

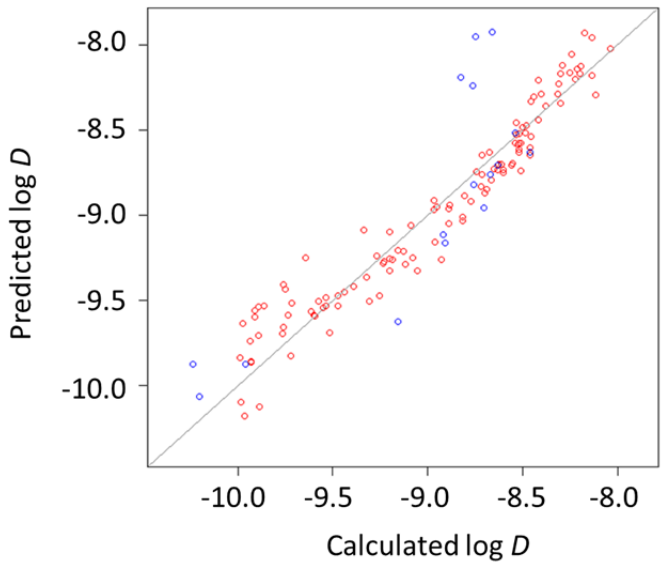

Figure 32. Comparison of predicted and calculated log *D* in PLSR

Table 5. Coefficients of all variables in PLSR. The values are after normalization of variables.

Vaiables	T	*Conc.*	*Mass*	*EA*	*IE1*	*IE2*	*IE3*
Coefficients	0.341	-0.338	-0.012	0.022	0.047	0.062	0.012
Vaiables	r	T_c	V	$Dis._{\text{Bi-Bi}}$	$Dis._{\text{Bi-}M}$	$Dis._{M\text{-}M}$	$Dis._{\text{Bi-O}}$
Coefficients	-0.064	-0.040	0.079	-0.138	0.149	0.070	-0.189
Vaiables	$Dis._{M\text{-O}}$	$Dis._{\text{O-O}}$	$CN_{\text{BiO}}(2.5)$	$CN_{MO}(2.5)$	$CN_{\text{BiO}}(3.2)$	$CN_{MO}(3.2)$	
Coefficients	-0.148	0.021	-0.357	-0.079	-0.016	-0.079	

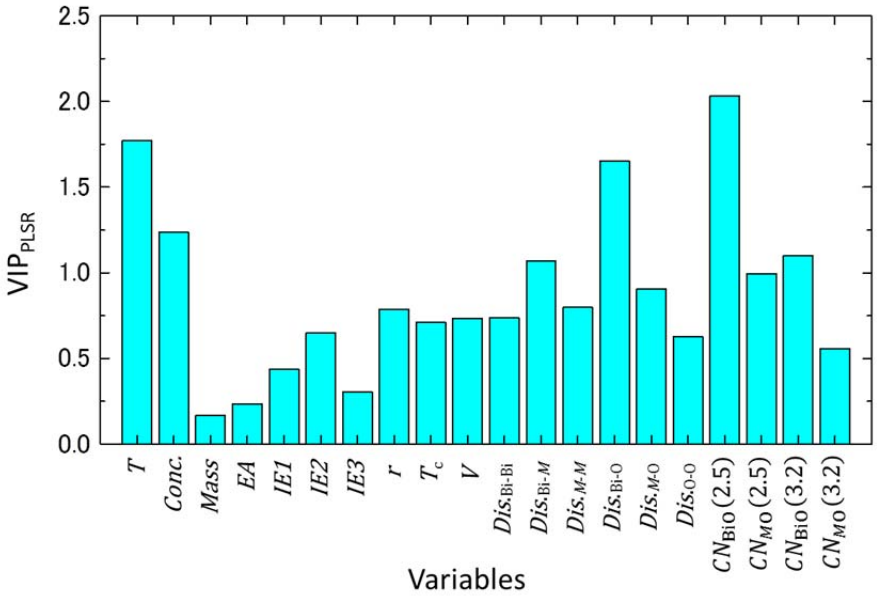

Figure 33. VIP_{PLSR} of all explanatory variables in the database

The RMSEs and the 5-fold CV scores of each method are summarized in Table 6. As the conclusion of these analyses, the PLSR reveals best regression for the data of the disordered structures and LASSO reveals best regression for the all data including the ordered structures. Moreover, the temperature and the concentration of *M* are most important to capture the characteristic of diffusion coefficients. Although this result is well known in disordered Bi_2O_3-M_2O_3 system, however, the characteristic of the ordered structures or more details cannot be captured only by them. Some methods, especially LASSO and PLSR, imply the importance of what are obtained from the radial distribution functions, average distance of Bi-O or $CN_{\mathrm{BiO}}(2.5)$ and they can explain diffusion coefficients of not only the disordered structures but also the ordered structures.

Table 6. RMSEs and 5-fold CV score of several methods in this analysis

Regression methods	RMSE of training data	5-hold CV score	RMSE of the data of ordered structures
OLSR with all variables	0.126	0.164	1.01
OLSR with AIC	0.134	0.145	0.316
OLSR with LASSO	0.155	0.162	0.213
PLSR	0.150	0.162	0.391

3-2-2. Prediction

In this section, we focused on the prediction of the logarithm of diffusion coefficients without MD simulations or with less time of them because it is high cost to perform MD simulations for a large space. As a result of section 3-2-1, the radial distribution function during MD simulation was indicated to be useful to predict the logarithm of diffusion coefficients. If the radial distribution function can be obtained by very short time MD simulation, diffusion coefficients can be predicted with an accuracy of section 3-2-1.

At first, we checked the convergence of the radial distribution functions. Figure 34 shows the time dependence of diffusion coefficient of pure Bi_2O_3 at 1100 K and the partial radial distribution functions up to several times. The partial radial distribution functions of Bi-O converged about one or two ps. However, the diffusion coefficients also converged at this time with almost same accuracy as that of section 3-2-1, about 0.15. Thus, the parameters of the partial radial distribution function cannot be used for the prediction of diffusion coefficients.

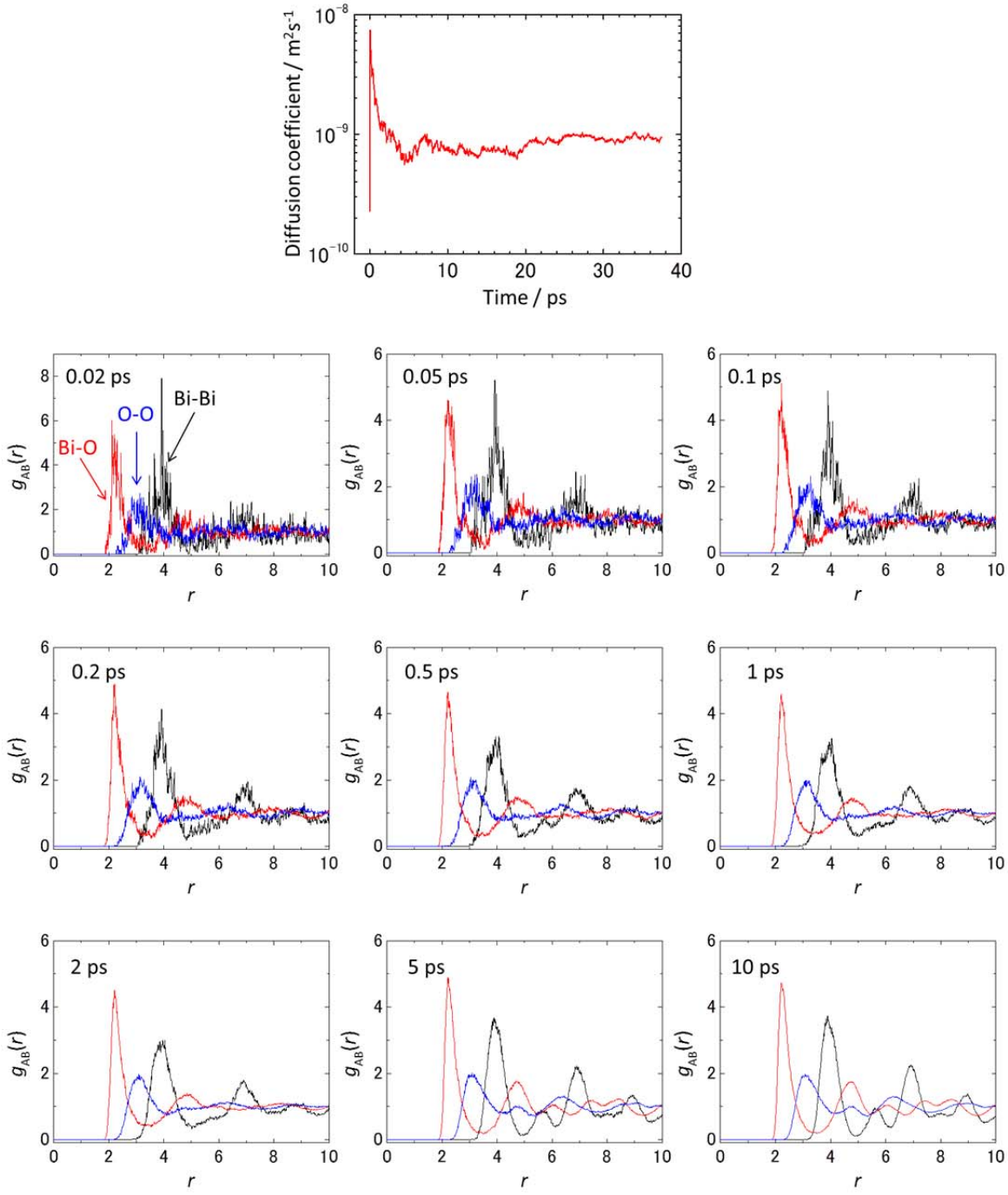

Figure 34. Time dependence of diffusion coefficient of pure Bi_2O_3 at 1100 K and the partial radial distribution functions up to several times

Table 7 shows the variables for prediction of the logarithm of diffusion coefficients. The parameters about the partial radial distribution functions are removed from the parameters in the analysis section. The data was divided into training data and test data for prediction. The RMSE of test data and 5-fold CV score mean whether regression is over-fitting or not. Moreover, the data was prepared and predicted in order to check predictive power of regression for the data which was not included to make regression. Further MD calculations were performed in a Bi-Tb system and we investigated whether their diffusion coefficients can be predicted. The results of the ordered structures were not predicted since they cannot be discriminated from disordered structures data by only the variables in Table 7. As prediction methods, OLSR with AIC, LASSO and PLSR were performed because they revealed good regression in the analysis section.

Table 7. Variables in prediction

Condition of MD	The temperature during MD	T
Property of M element	Concentration of M	*Conc.*
	Atomic mass of M	*Mass*
	Electron affinity of M	*EA*
	First, second, and third ionization energy of M	*IE1, IE2, IE3*
	van der Waals' radius of M	r
The property from systematic first-principles calculations	The order-disorder transition temperature (from chapter 2)	T_c
	Cell volume	V
The objective property	Logarithm of diffusion coefficients	$\log D$

Figure 34 shows the results of regressions. Red circles, blue circles and green circles mean training data, test data and the data of the Bi-Tb system, respectively. Since the order-disorder transition temperature of the Bi-Tb system was not calculated, the prediction of diffusion coefficients in this system could not be performed in PLSR, which need all of the explanatory variables of training data. Table 8 shows the RMSE of training dataset, the 5-fold CV score, the RMSE of test dataset, and the RMSE of the data of the Bi-Tb system. All methods can predict the logarithm of diffusion coefficients with an accuracy of 0.22 to 0.25. In all regressions, the diffusion coefficients around 10^{-10} m^2s^{-1} reveal high errors as shown in Figure 34. As one reason of this, it can be considered that the calculated diffusion coefficients have more errors in the area of small diffusion coefficients than other areas. The RMSE of the data of the Bi-Tb system is smaller than other RMSEs or CV score. This means that the constructed database is much suited for prediction of the Bi-Tb system and perhaps it may be possible to predict diffusion coefficients of bismuth and other rare-earth oxide solution systems.

The regression equations of OLSR with AIC and LASSO are given as following equation (28) and (29), respectively.

$$\log D = -0.022 + 0.91T - 0.52conc + 0.24V, \quad (28)$$

$$\log D = 0.77T - 0.44conc + 0.19V. \quad (29)$$

These two methods select the same variables, temperature, concentration and cell volume. Although this is adequate conclusion, however, it is surprising that with the accuracy of about 0.22 by only these three variables, the logarithm of diffusion coefficients in the Bi_2O_3-M_2O_3 systems can be predicted. Figure 35 shows these three parameters dependence of log *D*. The temperature and concentration dependence may be able to be captured from these figures, but volume dependence is difficult to be found. The search space, only disordered Bi_2O_3-M_2O_3 system, may be considered as the reason why these variables are selected. Only in this system, bismuth and rare-earth oxide system, the difference between *M* elements may be not so much and this difference is almost included in the parameter of cell volume. Although other parameters should be added if the ordered structures are considered, it is possible that the new important parameters are found by enlarging search space; other solutes elements or many other atom configurations.

Table 8. RMSEs and CV score of several methods in regression

Regression methods	RMSE of training data	5-hold CV score	RMSE of test data	RMSE of Bi-Tb system
OLSR with AIC	0.189	0.209	0.220	0.126
OLSR with LASSO	0.210	0.217	0.249	0.117
PLSR	0.185	0.212	0.230	–

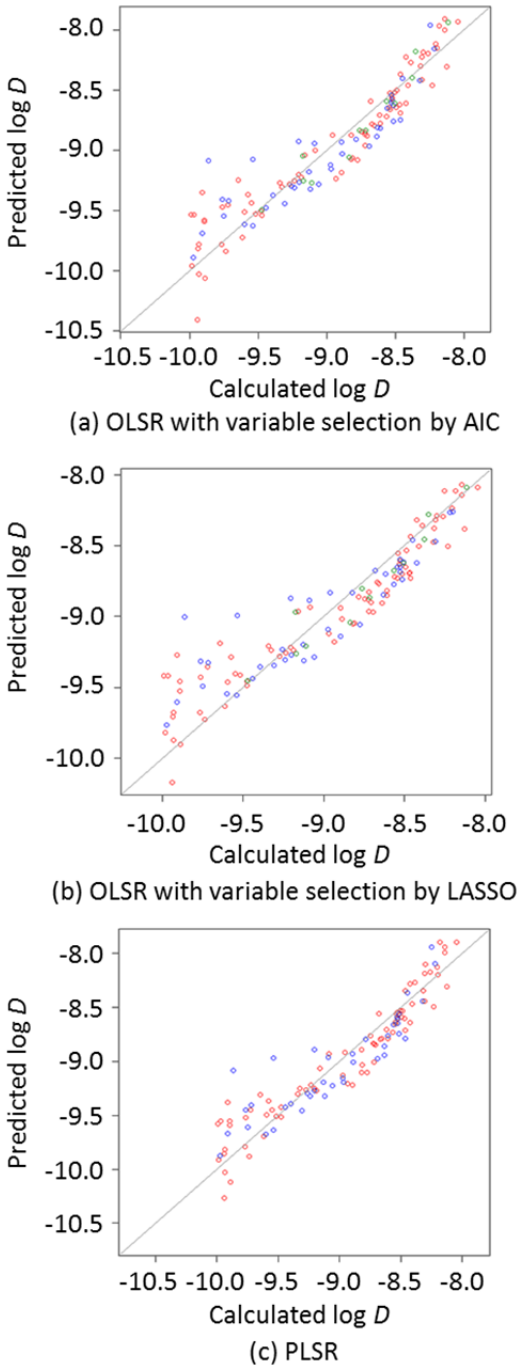

Figure 34. Comparison of predicted and calculated log *D* in (a) OLSR with variables selection by AIC, (b) LASSO, and (c) PLSR

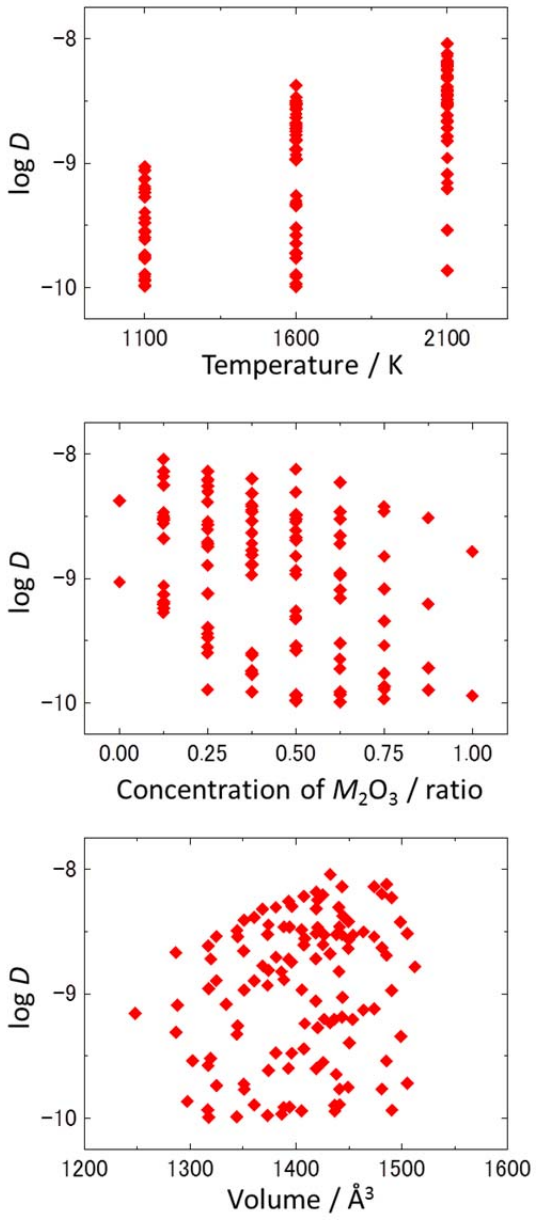

Figure 35. (a) Temperature, (b) Concentration, and (c) Volume dependence of log *D*

4. Conclusion

In this work, the first-principles MD simulation was performed in the Bi_2O_3-M_2O_3 systems (M=La, Nd, Sm, Gd, Dy, Y, Er, Lu) and the diffusion coefficients were calculated. The calculated diffusion coefficients agreed well with extrapolation of experimental ones, and the activation energies and the pre-exponential terms in Arrhenius equation also revealed good agreement with those of experiments. The diffusion coefficients tend to decrease with the increase of solutes concentration and ionic radii of solutes. In order to investigate the mechanism of the decrease of the diffusion coefficients, the partial radial and angular distribution functions were calculated.

The partial radial distribution functions in the solution systems indicated that solutes elements trapped oxide ion more strongly than bismuth. From the partial angular distribution functions, it was found that the local environments of oxide ion around solutes elements other than La and Nd were like the C-type rare-earth structure. These solutes oxides are known to exist as C-type rare-earth structure at ordinary temperatures and pressures. It is implied that these solutes trapped oxide ion and disturbed ion diffusion by oxide ordering like C-type rare-earth structure. On the other hand, La and Nd had other coordination environments and revealed higher diffusion coefficients than the solutes which preferred C-type rare-earth structures. Further calculations of the ordered structures revealed that the local environments depend on the configurations of cations as well as species of solutes.

In order to analyze the MD results, some informatics analyses were performed. The database in these systems was constructed from the results of MD simulations and the atomic parameters of solutes elements. It was found that the logarithmic of diffusion coefficients has linear relationship with concentration and temperature from the value of correlation coefficients. Moreover, the average distance of Bi-O or $CN_{\mathrm{BiO}}(2.5)$ from radial distribution functions have linear relationship with logarithmic of diffusion coefficients as well and this was also observed in the ordered structures. However, the partial radial distribution functions converged at almost same time as that of the diffusion coefficients and they could not be used for prediction of the diffusion coefficients. Thus, the regression for the prediction was performed using the database

without the parameters from the partial radial distribution functions. Only three parameters, temperature, concentration, and cell volume, were selected in the regression equation with an accuracy of about 0.22 of logarithm of diffusion coefficients. This prediction equation can be applied to the Bi_2O_3-Tb_2O_3 system which was not included in the data for regression. Although this equation is able to predict the diffusion coefficients only in disordered structures, the further additional parameters will be possible to make prediction with enough accuracy in other systems or ordered structures.

Reference

[1] P. Knauth and H. Tuller, J. Am. Ceram. Soc. **80**, 1654 (2002).

[2] A. M. Azad, S. Larose, and S. A. Akbar, J. Mater. Sci. **29**, 4135 (1994).

[3] H. A. Harwig and A. G. Gerards, Thermochim. Acta **28**, 121 (1979).

[4] T. Takahashi and H. Iwahara, Mater. Res. Bull. **13**, 1447 (1978).

[5] G. Gattow and D. Schütze, Zeitschrift Für Anorg. Und … **546**, (1964).

[6] P. D. Battle and C. R. A. Catlow, J. Phys. C: Solid State Phys. **16**, L561 (1983).

[7] M. Yashima and D. Ishimura, Chem. Phys. Lett. **378**, 395 (2003).

[8] C. Mohn, S. Stølen, S. Norberg, and S. Hull, Phys. Rev. Lett. **102**, 100 (2009).

[9] S. Hull, S. T. Norberg, M. G. Tucker, S. G. Eriksson, C. E. Mohn, and S. Stølen, Dalton Trans. 8737 (2009).

[10] A. Seko, Y. Koyama, A. Matsumoto, and I. Tanaka, J. Phys. Condens. Matter **24**, 475402 (2012).

[11] C. Mohn, S. Stølen, S. Norberg, and S. Hull, Phys. Rev. B **80**, 1 (2009).

[12] P. Shuk, H. D. Wiemhöfer, U. Guth, W. Göpel, and M. Greenblatt, Solid State Ionics **89**, 179 (1996).

[13] N. Sammes, G. Tompsett, H. Nafe, and F. Aldinger, J. Eur. Ceram. Soc. **19**, (1999).

[14] T. Takahashi, H. Iwahara, and T. Arao, J. Appl. Electrochem. **5**, 187 (1975).

[15] T. Takahashi, T. Esaka, and H. Iwahara, J. Appl. Electrochem. **5**, 197 (1975).

[16] M. J. Verkerk and A. J. Burggraaf, J. Electrochem. Soc. **128**, 75 (1981).

[17] M. Verkerk and K. Keizer, J. Appl. Electrochem. **10**, (1980).

[18] M. Yashima and D. Ishimura, Appl. Phys. Lett. **87**, 221909 (2005).

[19] M. Krynski, W. Wrobel, C. E. Mohn, J. R. Dygas, M. Malys, F. Krok, and I. Abrahams, Solid State Ionics **264**, 49 (2014).

[20] A. Jain, S. P. Ong, G. Hautier, W. Chen, W. D. Richards, S. Dacek, S. Cholia, D. Gunter, D. Skinner, G. Ceder, and K. a. Persson, APL Mater. **1**, 011002 (2013).

[21] S. Curtarolo, W. Setyawan, S. Wang, J. Xue, K. Yang, R. H. Taylor, L. J. Nelson, G. L. W. Hart, S. Sanvito, M. Buongiorno-Nardelli, N. Mingo, and O. Levy, Comput. Mater. Sci. **58**, 227 (2012).

[22] K. Momma and F. Izumi, J. Appl. Crystallogr. **41**, 653 (2008).

[23] I. Abrahams, X. Liu, S. Hull, S. T. Norberg, F. Krok, A. Kozanecka-Szmigiel, M. S. Islam, and S. J. Stokes, Chem. Mater. **22**, 4435 (2010).

[24] A. Zunger, S. Wei, L. Ferreira, and J. Bernard, Phys. Rev. Lett. **65**, 353 (1990).

[25] A. Seko, Y. Koyama, and I. Tanaka, Phys. Rev. B **80**, 1 (2009).

[26] S. Nosé, J. Chem. Phys. **81**, 511 (1984).

[27] S. Nosé, Prog. Theor. Phys. Suppl. (1991).

[28] P. Blöchl, Phys. Rev. B **50**, (1994).

[29] G. Kresse and D. Joubert, Phys. Rev. B **59**, 11 (1999).

[30] G. Kresse and J. Hafner, Phys. Rev. B **47**, (1993).

[31] G. Kresse and J. Furthmüller, Phys. Rev. B. Condens. Matter **54**, 11169 (1996).

[32] J. Perdew, K. Burke, and M. Ernzerhof, Phys. Rev. Lett. **77**, 3865 (1996).

[33] K. Rajan, C. Suh, and P. Mendez, Stat. Anal. Data Min. **1**, 361 (2009).

[34] I. Jolliffe, M. Uddin, and S. Vines, Clim. Res. **20**, 271 (2002).

[35] R. J. Morris, Acta Crystallogr. D. Biol. Crystallogr. **60**, 2133 (2004).

[36] P. Geladi and B. Kowalski, Anal. Chim. Acta **186**, (1986).

[37] T. Mehmood, H. Martens, S. Sæbø, J. Warringer, and L. Snipen, Algorithms Mol. Biol. **6**, 27 (2011).

[38] H. Akaike, in *Proc. 2nd Int. Symp. Inf. Theory* (Akadimiai Kiado, Budapest, 1973), pp. 267–283.

[39] R. Tibshirani, J. R. Stat. Soc. Ser. B (1996).

[40] P. Dey, J. Bible, S. Datta, S. Broderick, J. Jasinski, M. Sunkara, M. Menon, and K. Rajan, Comput. Mater. Sci. **83**, 185 (2014).

[41] W. N. Venables and B. D. Ripley, *Modern Applied Statistics with S*, 4th ed. (Springer, New York, 2002).

[42] H. A. Harwig, Bismuth Sesquioxide: Phase Relations and Electrical Properties, State University Utrecht, 1977.

[43] M. J. Verkerk and A. J. Burggraaf, Solid State Ionics **3-4**, 463 (1981).

[44] M. Faucher and J. Pannetier, Acta Crystallogr. Sect. B Struct. Crystallogr. Cryst. Chem. 3209 (1980).

[45] A. Ginya and I. Nobuhito, Chem. Rev. **98**, 1479 (1998).

Chapter 4

General Conclusion

In this thesis, the ionic conductivity in the Bi_2O_3-M_2O_3 systems (M=La, Nd, Sm, Gd, Dy, Y, Er, Lu) was investigated by systematic first-principles calculations. Main points of this thesis were summarized below:

In chapter 2, in order to obtain the knowledge about the deflection of ionic conductivity in Arrhenius plots, we predicted the order-disorder transition temperature in the δ-Bi_2O_3-M_2O_3 systems, considering that the deflection is due to the order-disorder transition of oxide ion sublattice. The order-disorder transition temperature T_c was predicted by estimating the free energies of the ordered and disordered structures. We propose the special structures search based on the cluster expansion method to estimate the ground state ordered structure's energy efficiently. The predictive potential of the special structures search was demonstrated in pure δ-Bi_2O_3. The ground state ordered structure can be obtained by calculation only for the special structures. Then, T_c of pure δ-Bi_2O_3 was predicted. The predicted T_c was consistent with the experimental β-δ transition temperature, which can be assumed as the oxygen order-disorder transition temperature in this work. The predicted T_c in the Bi_2O_3-M_2O_3 systems represents good agreement with the deflection temperature of ionic conductivity. This result suggests that the deflection of ionic conductivity is due to order-disorder transition of oxygen sublattice. Our method can reduced the number of calculation structures drastically and it is easy to apply many other systems involved in order-disorder transition.

In chapter 3, the first-principles molecular dynamics was performed in Bi_2O_3-M_2O_3 systems (M=La, Nd, Sm, Gd, Dy, Y, Er, Lu) and the diffusion coefficients were calculated to elucidate the origin of the decrease of ionic conductivity at higher temperature than they deflection point with the increase of concentration of solutes. The calculated diffusion coefficients agreed well with extrapolation of experimental ones, and the activation energies and the pre-exponential terms in Arrhenius equation also revealed good agreement with those of experiments. In order to investigate the

mechanism of the decrease of the diffusion coefficients, the partial radial and angular distribution functions were calculated. The partial radial distribution functions in the solution systems indicated that the solutes elements trapped the oxide ion more strongly than bismuth. From the partial angular distribution functions, it was found that the local environments of oxide ion around solutes elements other than La and Nd were similar with C-type rare earth structure. These solutes oxides are known to exist as C-type rare-earth structure at ordinary temperatures and pressures. The solutes trapped oxide ion and disturbed ion diffusion by oxide ordering like C-type rare-earth structure. On the other hand, La and Nd had other coordination environments and revealed higher diffusion coefficients than the solutes which preferred C-type rare-earth structures. Further calculations of the ordered structures revealed that the local environments also depend on the configurations of cations.

In order to analyze these results, some informatics analyses were performed. The database in these systems was constructed from the results of molecular dynamics and the atomic parameters of solutes elements. It was found that the logarithmic of diffusion coefficients has strong linear relationship with the concentration and temperature. Moreover, the average distance of Bi-O or $CN_{\mathrm{BiO}}(2.5)$ from the partial radial distribution functions has linear relationship with the logarithmic of diffusion coefficients. This consists also in the data of ordered structures. However, the radial distribution functions converged at almost same time as that of the diffusion coefficients and the parameters from them could not be used for the prediction of the diffusion coefficients. Thus, the regression for the prediction was performed using the database without the parameters from the partial radial distribution functions. Using only three parameters, the temperature, the concentration, and the cell volume, diffusion coefficients could be predict with an accuracy of about 0.22 of logarithm. This regression equation can predict the diffusion coefficients in the Bi_2O_3-Tb_2O_3 system whose data was not used for the regression. Further additional parameters will be possible to make the prediction with enough accuracy in other systems or ordered structures.

According to this thesis, the mechanism of ionic conductivity was elucidated in the Bi_2O_3-M_2O_3 systems. Subsequently, the possibility to estimate ionic conductivity was demonstrated in these systems by systematic first-principles calculations. We

expect that the results of this thesis will lead to new material design of ionic conductor with cubic Bi_2O_3 structure in near future. Moreover, it is expected that the methods like this thesis will be applied to many other properties of materials.

Acknowledgement

The author would like to express his deepest gratitude to Professor Isao Tanaka at Kyoto University for continuous guidance and encouragement throughout this work. The author wishes to express his gratitude to Associate Professor Fumiyasu Oba for his for helpful discussions and advice. He would like to thank Associate Professor Atsuto Seko for his continuous helpful discussions and advices throughout this work. The author gratefully shows his appreciation to Associate Professor Yukinori Koyama for his fruitful discussions thorough out this work. The author wishes to express his deepest gratitude to gratitude to Professor Tetsuya Uda and Yasuharu Shirai for their critical reading of this thesis.

The author would like to express his gratitude to Professor Krishna Rajan at Iowa State University for his helpful discussion of informatics analysis technique. The author would like to express his gratitude to Associate Professor Scott Broderick for his helpful advice of useful regression technique.

The author would like to express his gratitude to Associate Professor Atsushi Togo for wide range of his helpful advice of supercell search for the calculations. The author would like to express his gratitude to Yoyo Hinuma for his helpful advice of estimation the energies. The author would like to express his gratitude to Dr. Yu Kumagai for his helpful advice of first-principles calculations. The author would like to express his gratitude to Dr. Hiroyuki Hayashi for his helpful discussion in the view point of experimental view. The author would like to express his gratitude to Dr. Masahiro Mori for his helpful discussion of first-principles calculations. The author would like to express his gratitude to Dr. Yuji Ikeda for his helpful discussion of special quasirandom structures. The author would like to express his gratitude to Dr. Lee Joohwi for his helpful discussion of regression technique. The author would like to express his gratitude to Mr. Shota Katayama for his helpful discussions and encouragement in the laboratory life.The author wishes to make grateful acknowledgement to the members of Professor Tanaka’s group for helpful discussions throughout this work. Especially, he would like to thank Ms. Makiko Orita for her a lot of helps.

Finally, the author would like to sincerely thank his family for their enduring support and encouragement.